CHALMERS

Radio channel measurement in 3G networks

Master of Science Thesis

SEPIDEH AFSARDOOST

Department of Signals and Systems
Division of xxx
CHALMERS UNIVERSITY OF TECHNOLOGY
Göteborg, Sweden, 2009
Report No. EX027/2009

CHALMERS ERICSSON

Radio Channel Measurement in 3G Networks

Sepideh Afsardoost

Master of Science Thesis

Antenna Systems and Propagation
Access Technologies and Signal Processing
Ericsson Research
Ericsson AB

and

Communication System Group
Department of Signal and Systems
Chalmers University of Technology

May 2009

EX027/2009

Supervisor:

Henrik Asplund
Access Technologies and Signal Processing
Ericsson Research, Ericsson AB
Kista, Sweden

Examiner:

Erik Ström
Signals and Systems
Chalmers University of Technology
Göteborg, Sweden

ABSTRACT

Many of the current channel models used in research and development of cellular systems have been developed based on channel measurements not performed in real networks. Instead, in these measurements some dedicated equipments have been mounted in locations of prospective network deployments to represent the actual networks. Moreover, these measurements have been conducted in conditions representing few large cells. As the uptake of mobile devices has accelerated, the cellular networks have consequently turned out to be denser with many small cells. Hence, it has been questioned if the channel models are still representative of the present network deployments.

In this thesis, the time dispersion characteristics of different channel environments including urban, suburban, rural and highway have been studied. Two major channel measurement campaigns have been performed in Stockholm and Atlanta covering the mentioned environments while measurements on a smaller scale have been performed in France and New Orleans. All the measurements have been performed within live 3G networks belonging to different operators. The measurement data have been processed and analyzed with special focus on rms delay spread of the channels. Statistical approaches have been employed throughout the work to analyze the data and compare the results.

The channel measurements accuracy of the utilized 3G phone has been verified by controlled lab measurements to make certain that the results are trustful. Some currently used channel models have been compared to the measurement results. Moreover, the relationships of pairings rms delay spread vs. base-mobile distance, rms delay spread vs. Received Signal Code Power (RSCP) and RSCP vs. base-mobile distance have been studied. Another considered matter in this work is finding the correlation of rms delay spread within and between the sites of the cellular networks.

The analysis indicates that the median value of the rms delay spread is typically about $0.2\mu s$ which is smaller than that of experienced in our considered channel models. It is shown that Spatial Channel Model (SCM) suburban model was the only model fitted well to the data. Also, the measured data did not show noticeable relationship neither between rms delay spread and base-mobile distance nor between rms delay spread and RSCP. However, RSCP vs. base-mobile distance has followed the Log-distance pathloss model and the pathloss exponents of Stockholm and Atlanta were estimated. Moreover, a slight correlation between the rms delay spreads originated from the same site was noticed.

ABREVIATIONS

3G	3rd Generation
3GPP	3rd Generation Partnership Project
BS	Base Station
DS-CDMA	Direct Sequence-Code Division Multiple Access
GE	Google Earth
GMT	Greenwich Mean Time
GPS	Global Positioning System
PN	Pseudo Noise
PSC	Primary Scrambling Code
RA	Rural Area
RRC	Radio Resource Control
RSCP	Received Signal Code Power
SC	Scrambling Code
SCM	Spatial Channel Model
SNR	Signal-to-Noise Ratio
TU	Typical Urban
WCDMA	Wideband Code Division Multiple Access

CONTENTS

1 INTRODUCTION 1
1.1 Background 1
1.2 Purpose 1
1.3 Thesis Outline 2
2 MEASUREMENTS 3
2.1 Measurement Technique 3
2.1.1 DS-CDMA 3
2.1.2 WCDMA 3
2.1.3 Rake Receiver and Path Searcher 4
2.2 Measurement Equipment 6
2.3 Measurement Outputs 6
2.3.1 Path Searcher Outputs 7
2.3.2 GPS file output 9
2.4 Measurement Scenario 10
2.4.1 Google earth images 13
3 ANALYSIS 15
3.1 Channel estimates verification 15
3.1.1 Averaging the power delay profiles 16
3.1.2 Two-tap channel 17
3.1.3 Channel A (2.72 km/h) 18
3.1.4 Channel A (100 km/h) 20
3.1.5 Typical Urban channel (TU) 21
3.1.6 Rural Area channel (RA) 22
3.1.7 Pedestrian A channel 23
3.2 Initial Data Analysis 25
3.2.1 Pre-processing 25
3.2.2 Geographical coordinate assortment 26
3.2.3 Cell assortment 28
3.3 Analysis results 29

3.3.1 The distribution of the rms delay spread....33
3.3.2 Results comparison with channel models....40
3.3.3 Forest effect on delay spread....43
3.3.4 rms delay spread versus base-mobile distance....45
3.3.5 rms delay spread versus RSCP....49
3.3.6 RSCP versus base-mobile distance....50
3.3.7 Correlation of delay spread within and between sites....55
4 CONCLUSIONS AND DISCUSSION....58
4.1 Future work....58
APPENDIX A....60
REFRENCES....65

1 INTRODUCTION

1.1 Background

In order to design, simulate and plan the wireless systems, the channel models are extensively used. Such models are very desirable mostly because they reduce both the cost and time of evaluating and simulating a practical communication system. Besides, the channel models highlight the important properties of propagation channels. These are the properties which have an impact on system performance.

However, the channel parameters are obtained from extensive measurement campaigns in any channel model which is based on measurement data. These measurements are performed by different channel sounding equipments, each capable of measuring different channel parameters e.g. impulse responses, field strength and etc. Moreover, the characteristics of every type of environment have to be determined through experimental measurements. Once the measurements have been performed, a suitable channel model which fits well to the data can be constructed.

Many of these measurements are performed in networks with a few large cells. These measurements leaded to variety of standardized channel models which were widely used in research and development to develop new products and also in deployment of cellular systems. However, the increasing demand of mobile utilizations in the last decade has led to more and more cells added to the cellular networks making them denser with a large number of small cells. Consequently, the cellular systems have changed whereas the channel models remained the same.

Therefore, whether the currently used channel models represent the current network deployment has been called into question. Specifically, the 3G network propagation models have become the focus of interest. To answer this question, we have performed several measurement campaigns within 3G networks to analyze the measured channel with an emphasis on time dispersion and compare the results with existing channel models in use.

1.2 Purpose

The purpose of this thesis is:

- Performing channel measurements in different environmental types
- Analysis of the measured channels with special emphasis on the time dispersion
- Evaluating the channel models used in research and development
- Find the possible relationships among the rms delay spread, the base-mobile distance and the Received Signal Code Power (RSCP)

1.3 Thesis Outline

This report consists of two major sections: section 2 and section 3 which respectively describe the measurement and analysis phases of the thesis. In section 2, the used measurement technique, equipments and output parameters are described. Also, the detailed measurement scenario is presented at the end of this section. Section 3 begins with evaluating the channel estimates. It then follows with describing the data processing. The analysis results are all presented at the end of this section. The conclusions that can be drawn from the analysis results are summarized in section 4 where some suggestions for future work are also presented.

2 MEASUREMENTS

2.1 Measurement Technique

Channel measurements can be performed either by transmitting a short radio frequency pulse and receiving the signal from different paths, or by transmitting a wideband spread-spectrum signal which consists of a sequence of bits enabling pulse transmission [1]. The later method gives rise to a larger coverage and thus is more appropriate for outdoor measurements as we are interested in. In practice, a DS-CDMA system is used to carry out the pulse transmission.

2.1.1 DS-CDMA

DS-CDMA (Direct-Sequence Code Division Multiple access) is a technique in which information bits are spread in a bandwidth which is much wider that the original signal bandwidth. This task is accomplished by multiplying every information bit with a Pseudo Noise (PN) sequence having a higher bandwidth. A PN sequence or spreading code is a sequence of ± 1 bits each called chip.

Therefore, every data bit is repeated N times where N is spreading factor. The spreading factor is proportional to the ratio of the chip rate and bit rate. Hence: $N = R_c / R$ where R_c is chip rate and R is the bit rate.

The receiver must know the correct spreading code sequence to collect the actual data bit by de-spreading from the N chips. The PN sequences should be orthogonal to each other meaning that the cross-correlation between every two of them is almost zero.

2.1.2 WCDMA

Since the measurements are performed in WCDMA networks, we present some features of this system here. WCDMA is a wideband DS-CDMA, i.e. the user information bits are spread over a large bandwidth. The chip rate in WCDMA is $3.84 Mcps$ leading to a carrier bandwidth of $5 MHz$. This chip rate gives the chip duration of $0.26 \mu s$, so the WCDMA receiver can resolve and combine the multipath components with time difference of larger than $0.26 \mu s$.

WCDMA uses two code types; Spreading code or Channelisation code which spreads out the data bits into $5 MHz$ as described for DS-CDMA, and Scrambling codes (SC) which uniquely identify the transmitter. Scrambling is used after spreading and, in contrast to the spreading, does not change the signal bandwidth and only makes the signal from different terminals and Base Stations (BSes) separable. The figure below shows this coding process [6].

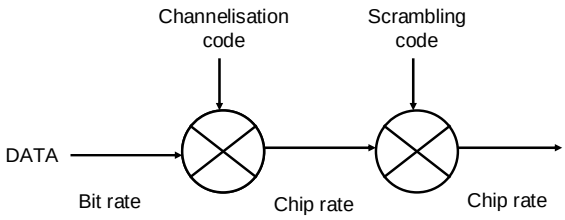

Figure 2-1: coding process in WCDMA

In WCDMA, channelisation codes are used to distinguish between different channels from a BS, while SCes are used to distinguish between different BSes.

2.1.3 Rake Receiver and Path Searcher

In WCDMA, Rake receiver is the most commonly used receiver. A Rake receiver is a matched filter receiver designed to detect resolvable multipath component. It consists of several taps, Rake fingers, which are allocated to each multipath component. Hence the received signal energy is maximized and the effect of fading on transmission is mitigated. In other words, if there are D different resolvable multipath components, the Rake receiver may increase the performance by a D-order diversity system. Figure 2-2 shows a simple Rake receiver scheme.

A path searcher determines the delays before descrambling and updates the Rake receiver with new paths and delays. The path searcher keeps track of the peaks in an estimated channel impulse response to find the new paths.

In the coherent based scheme of the path searcher, known pilot symbols are sent in the transmitter. At the receiver end the channel estimation algorithm can estimate the transmission channel with an operation on received signal along with the known symbols. The received signal $r(n)$ is cross-correlated with a delayed complex conjugated local replica of the PN sequence used in the transmitter $p^*(n-k)$. The cross-correlation is performed over N chips. The result of the cross-correlation shows to what extent the received signal and the shifted PN sequence are similar. If the cross-correlation is high enough at a specific phase shift which is made by changing the k, there should be a new path and this new path can be assigned to a Rake receiver finger. The figure 2-3 demonstrates how path searcher assigns delay estimates to Rake fingers.

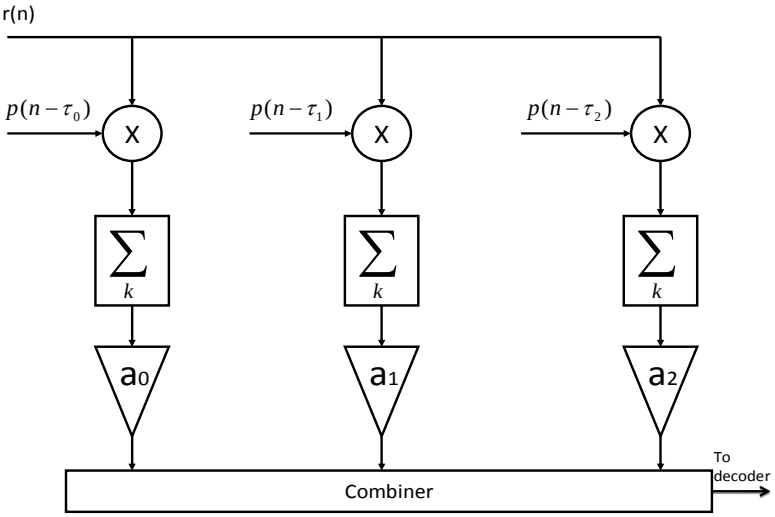

Figure 2-2: Rake receiver

Therefore, the path searcher tests whether a ray at a particular phase is present or not. Also, the path searcher looks for multipath rays by a N_w long window over the whole WCDMA frame with a length of 34800 chips.

The mathematical expression for the cross-correlation is given below. In order to obtain a real decision variable, the absolute value of the cross-correlation is squared.

$$z(k) = \left| \sum_{m=0}^{N-1} r(m) p^*(m-k) \right|^2 \quad (1)$$

Where $r(n) = r_I(n) + jr_Q(n) \quad p(n) = p_I(n) + jp_Q(n)$

If the result is higher than a threshold, the path searcher assigns a new delay path to a Rake finger.

After the path searcher assigns the Rake fingers, the following steps occur in a WCDMA receiver.

1. Descrambling: the received signal is multiplied by the SC and delayed versions of it to find out from which BS the signal is sent.
2. Despreading: the descrambled signal of each path is then multiplied with the spreading code to despread the signal.

3. Integration and combining: the despread signal of each path is integrated over one symbol time and the output signals of all paths are then combined using the estimated channel information and a combining scheme such as MRC.

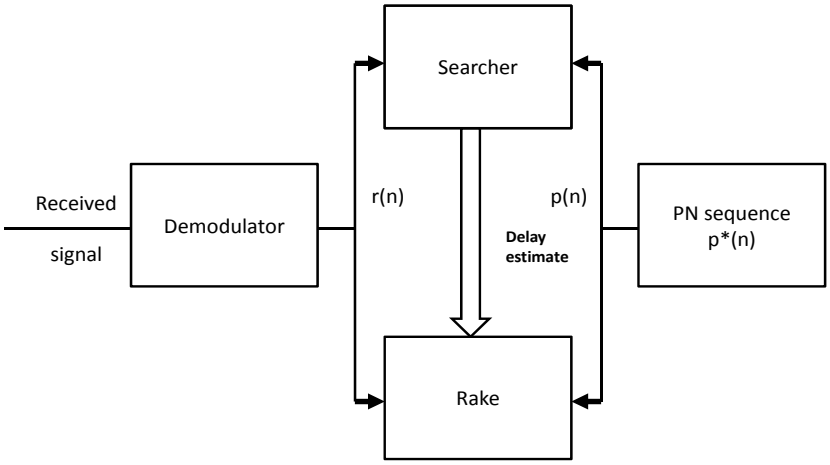

Figure 2-3: path searcher assigns delay estimates to Rake fingers

2.2 Measurement Equipment

The equipment used to measure the channel is a 3G mobile phone, which is capable of logging output from the path searcher. The mobile phone is connected to a portable computer and the log files are stored in the computer as long as measurement is carrying on. Furthermore, one GPS device is also connected to the computer so that GPS information of the measured routes is also stored in a separate file. Later, both the path searcher log file and the GPS file are parsed in order to extract the required data and to perform further analysis in next stages. Figure 2-4 shows a scheme of equipments we have used in the measurements.

2.3 Measurement Outputs

As mentioned before, there are two main measurement output files. One output file is a log file of the path searcher outputs, the other one is a GPS file which presents GPS data of the measurement routes and regions.

Figure 2-4: measurement equipments

2.3.1 Path Searcher Outputs

Path searcher output is recorded instantaneously in the log file. Each record is marked with a timestamp and a counter which presents the number of seconds after midnight. The timestamps are derived from the computer time. These timestamps enable us to keep track of the records.

The recorded logs are either the path searcher channel impulse responses or RRC (Radio Resource Control) measurement reports. However, all of them are stored in one unique text file but with their particular labels so that they can be extracted separately while parsing the text file.

The main interesting outputs of the path searcher are the instantaneous channel impulse responses of the channel which are sampled and recorded with different chip resolutions. In fact, multipath delays are not quantized to the chip rate. So, it is sometimes beneficial to over-sample the power delay profiles. An example of such an impulse response is shown in figure 2-5.

It is worth mentioning that the first tap in the channel impulse response is considered with delay 0 ($\tau_1 = 0$), and the other tap delays are computed based on the first one. Also, the delay difference between taps can give the difference in multipath length. The example shown in figure 2-6 clarifies this issue. The delay time between two taps indicated by arrows is $\tau_1 - \tau_0$ which shows they are derived from two multipath components with length difference of $(\tau_1 - \tau_0) \cdot c$ meters, where c is the speed of the light.

In addition to the channel impulse response, the Primary Scrambling Code (PSC) of the corresponding cell is logged in the file. Thus, we can assign each receiving channel impulse to its relative transmitting cell.

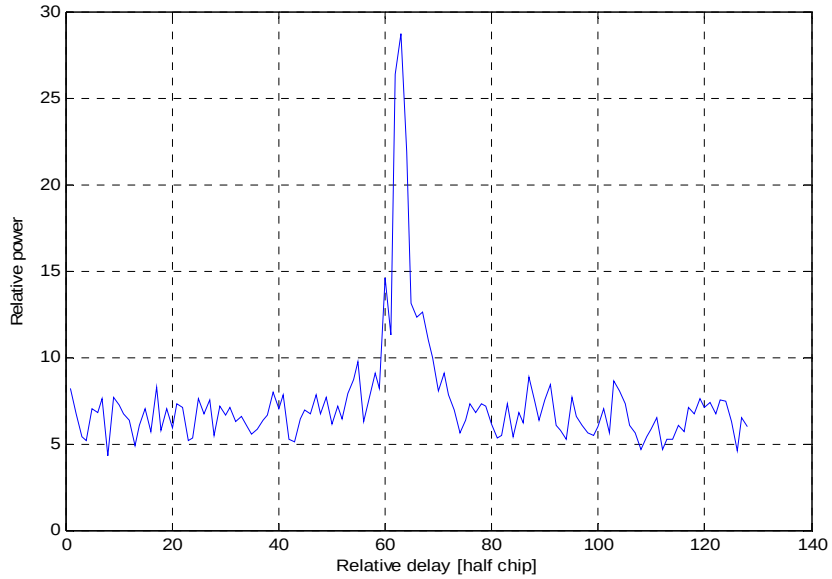

Figure 2-5: Example of an impulse response

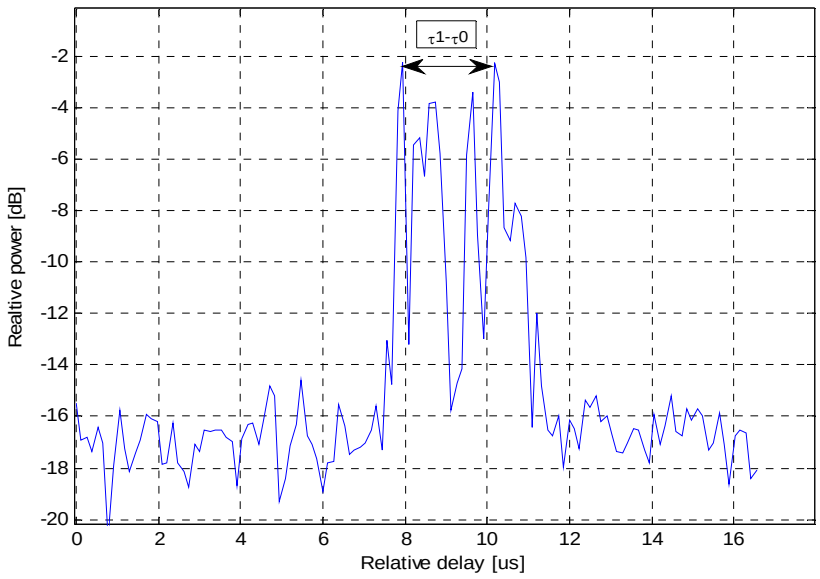

Figure 2-6: the delay time $\tau_1 - \tau_0$ is derived from two multipath components with length difference of $(\tau_1 - \tau_0) \cdot c$ meters

The RRC measurement report is another type of record in the log file. It instantaneously reports the SCes of all receiving cells with their corresponding Received Signal Code Power (RSCP) that is the received power on each SC after despreading. One sample of RSCP values received from 3 different cells in a 37 seconds measurement is illustrated in the figure2-7.

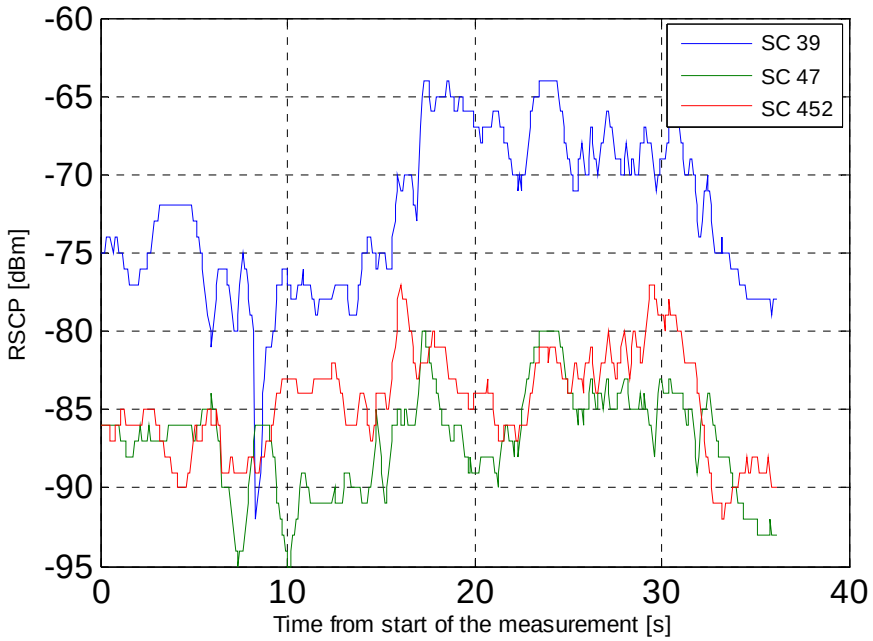

Figure 2-7: one sample of RSCP values received from 3 different cells in 37 seconds

2.3.2 GPS file output

One GPS (Global Positioning System) device is included in the measurement equipment to store the geographical information of the measurement campaigns. This GPS device stores some important properties of the measured routes such as longitudes and latitudes. Longitude and latitude give the geographical coordinates of the routes. Besides, every GPS coordinate is tagged with GPS time which is matched to Greenwich Mean Time (GMT). However, it should be noted that log counter time is synchronized with the laptop time that is usually set to local time, while the GPS time is synchronized with GMT.

Longitude gives the location of a place on east or west of the prime meridian and is given in angular format ranging from $0°$ at the prime meridian to $+180°$ eastward and $-180°$ westward. Lines of longitude are vertical on maps.

Latitude gives the location of a place on earth north or south of the equator. Lines of latitude are the horizontal lines shown running east to west on maps. Technically, latitude is also in degrees ranging from $0°$ at the equator (low latitude) to $90°$ at the poles ($90°N$ for the North Pole or $90° S$ for the South Pole).

Each degree of longitude or latitude is divided into 60 minutes, each of which divided into 60 seconds. Thus, a longitude or latitude can be expressed respectively by a notation as $23°27'30"E$ or $23° 26' 21" N$. An alternative representation uses degrees and minutes, where parts of a minute are expressed in decimal notation with a fraction, thus: $23°27.500'E$ *or* $23° 26.350'N$.

The original GPS coordinates obtained from our GPS equipment is in this format. But, on the purpose of calculation it is preferred to convert them to decimal format such as $23.45833°E$ or $23.439167°N$. Also, the West/East suffix can be replaced by a negative sign for western hemisphere and North/South suffix can be replaced by a negative sign for south hemisphere.

2.4 Measurement Scenario

The measurement setup was designed to provide enough data to enable us to extract the typical behavior of the channels in environments such as urban, sub-urban, highways and rural areas. The measurements were carried out while driving by car using the test terminal inside the car.

Stockholm and Atlanta [1]were mainly targeted to perform the measurements. Atlanta as an American city has different city structure than the European city of Stockholm. The downtown of Atlanta has a heterogeneous structure with high variations in building structures. The buildings have various height levels with popping up skyscrapers. The suburban area has lower density compared with urban with homogenous residential buildings. On the other hand, the urban area of Stockholm has also dense but homogenous structure with mostly medium-height buildings. There are fewer high-rise buildings in Stockholm than in Atlanta with also lower height level. The suburban in Stockholm is almost similar to that of Atlanta.

Several hours in various days were dedicated to cover urban, suburban and rural areas in Stockholm, and also urban, suburban and highways in Atlanta. The measurements were performed in networks of one of the operators in Stockholm and a different operator in Atlanta. In addition to Stockholm and Atlanta, two other measurement campaigns have been performed in France (Lille) [2]and New Orleans[3] on a smaller scale.

---

[1] Performed by Henrik Asplund

[2] Performed by Henrik Asplund

[3] Performed by Yngve Selén

The measurements in New Orleans were mainly performed in the famous "French Quarter" area which has quite old European style. So, all mentioned cities can be put into two main groups based on their city styles. Atlanta in one group as it has American city structure, and Stockholm, Lille and New Orleans in another groups due to their European style. The following figures are some skylines of these cities to better describe their city structure.

Figure 2-8: Stockholm skyline

Figure 2-9: Atlanta skyline

Figure 2-10: Lille skyline

Figure 2-11: New Orleans French Quarter skyline

The table below gives more details regarding the approximate dedicated time, the covered route length and the approximate number of power delay profiles for each area in each city.

City	Covered areas	Approx. hours	Route length(km)	Approx. pdps
Stockholm	Urban	5.5	100	220000
	Suburban	5.5	210	200000
	Rural	1.5	90	42000
Atlanta	Urban	2	75	100000
	Suburban	7.8	300	348000
	Highways	1	90	40000
Lille	Urban	1.5	50	75000
	Highways	1	60	50000
New Orleans	Urban	1.2	20	68000
Total	-	27	995	1143000

Table 2-1: measurement scenario: name of the cities

2.4.1 Google earth images

Google earth (GE) provides some interesting features which turned out to be very useful in this thesis work. One of the primary features is to illustrate the routes in the GE by knowing the GPS coordinates of the routes. Also, by knowing the cell site coordinates one can demonstrate the BSes locations in GE. Moreover, in later stages, the data analysis results will be used to present the data values by color coded paths in GE.

In GE, a file format, KML, is used to display the geographical data. The KML uses tag based structures and is based on the XML standard. The KML files can be created in text editors from scratch. Variant styles and structures can be used in this file format to create the desired geographical display. The KML documentations and references provided by GE are helpful guides in this regard.

Different objects can be placed on the earth surface by a Placemark. A Placemark can be a path or an icon or other geometry elements. For example, icons are used to mark the BSes, while paths are used to demonstrate the measurement paths in our

case. Both paths and icons can have different styles and different colors which are all definable by line or icon styles and color codes. The GPS coordinate should also be tagged by the tag Point in the Placemark to show the icon or path. There should be at least two coordinates to create a path because the coordinates connect to each other in paths, while it is not the case for an icon.

The measured routes in different areas of Stockholm, Atlanta, France and New Orleans are illustrated in figures of appendix A.

As it was mentioned, the data values can also be illustrated in GE by color coded paths. Later, we will use this feature to show our measurement data values in the whole way in which measurement has been taken with different colors corresponding to different values at each coordinate.

The scripts creating these files employ KML file formats in combination with the GPS coordinates and the relative numerical values of the data. Indeed, the color coded paths consists of icons colored based on their given values. To map the colors from Matlab to KML, 64 color codes are defined based on the 64 colormap steps of Matlab. Both KML and Matlab use RGB color systems. But the color values are within [0 1] interval in Matlab, while they are within [00 FF] in hexadecimal in KML.

Therefore, while plotting each GPS coordinate in GE, its relative color code based on its numerical value, is called to represent the value. Some sample images of these GE paths will be used in later sections.

3 ANALYSIS

One purpose of the measurement data analysis is to present the multipath characterization of cellular channels in 3G networks. One very defining index of multipath dispersion is rms delay spread, σ_{Tm} which is the square root of the second central moment of the power delay profile. The mathematical expressions of mean delay spread and the rms delay spread are as follows:

$$\mu_{Tm} = \frac{\int_0^\infty p(\tau).\tau d\tau}{\int_0^\infty p(\tau) d\tau} \qquad (1)$$

$$\sigma_{Tm} = \sqrt{\frac{\int_0^\infty (\tau - \mu_{Tm})^2 . p(\tau) d\tau}{\int_0^\infty p(\tau) d\tau}}$$

Where τ is the delay time and $p(\tau)$ is the power of each delay. The rms delay spread represents the effective value of the time dispersion of transmitted signal, as caused by the multipath in the channel. To have a reliable transmission channel, the time duration of each transmitted symbol should be much longer than rms delay spread value in order to minimize the distortion of the symbol shape observed at the receiver. Thus: $T >> \sigma_{Tm}$ where T is the symbol duration.

Moreover, since the duration of a transmitted symbol is inversely proportional to the data rate, the inverse of the rms delay spread can be considered as a measure of the data rate limitations of a fading multipath channel [1]. However, if a system employs an equalizer or other anti-multipath techniques such as CDMA, it can operate reliably with symbol duration near the rms delay spread.

Hence, the rms delay spread is probably one very significant single measure of multipath dispersion in a multipath fading channel. However, the quality of the measurements and channel estimates should be first assessed to rely on the data analysis results as section 3.1 will explain. Section 3.2 describes the initial data analysis including data pre-processing, data classification and data summarizing. Section 3.3 is analysis results.

3.1 Channel estimates verification

The accuracy of channel estimates was evaluated by lab measurements. In the lab, the measurement equipment was connected to one single BS via a channel emulator for which different channel models were defined. The channels chosen to evaluate the channel estimates are Pedestrian channel (Ped A), Typical Urban channel (TU),

Rural Area channel (RA) and two arbitrary channels which are two-tap channel and channel A. All channels are considered case by case in the 3.1.2 to 3.1.7 sub-sections.

The power delay profiles of each channel were assessed and compared both in terms of shape and in terms of rms delay spread to the channel model. The comparison in terms of shape is possible by having the averaged power delay profile. Averaging the measured power delay profiles is described in the following section.

3.1.1 Averaging the power delay profiles

In order to obtain the average of instantaneous measured power delay profiles, one problem arises. The problem is caused by the misalignment of instantaneous power delay profiles. The instantaneous power delay profiles are truncated from a WCDMA frame with a length of 38400 chips so that the most energized part of the signal is centralized in a shorter frame. Therefore, the power delay profiles are not always synchronized. To align the power delay profiles, one method is to find the number of the chip (start point) from which the power delay frame is truncated. This start point is recorded in the log file. Hence, by extracting this parameter for all power delay profiles and shifting them based on their starting point's differences, one can align the power delay profiles.

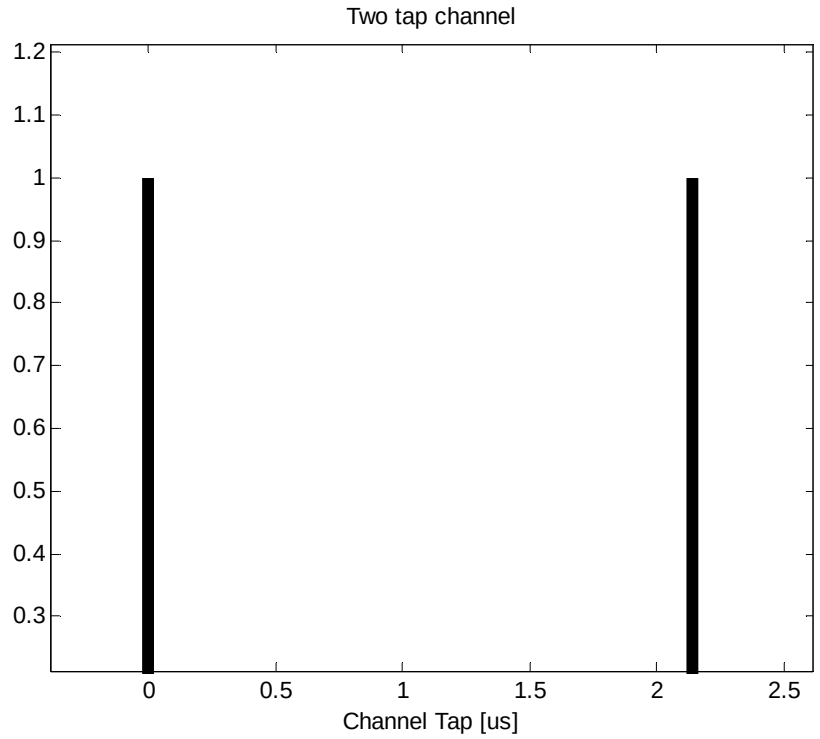

Figure 3-1: two-tap channel

However, after applying this method there was still a very slight misalignments in some places which can be due to the original misalignment of the WCDMA frames. To align the power delay profiles even better, cross correlation can be useful, i.e. detecting the highest peak of the cross correlation between the first power delay profile as a reference and the rest of the profiles can indicate if there is any shift between the reference and the power delay profiles.

However, in our case, the power delay profiles can be distorted due to the fading and the highest peak does not consistently indicate when the most similarity occurs. Hence, cross correlation did not work as expected in our case. As the misalignments were quite a few, the best way was simply to fix them manually.

3.1.2 Two-tap channel

Two-tap channel is one of the arbitrary channels defined to evaluate the channel estimates. Figure 3-1 shows this channel which has two equal power taps. The delay between the taps is $2.14\mu s$ and the power of each tap is $0dB$. The vehicular speed was set to $2.72km/h$.

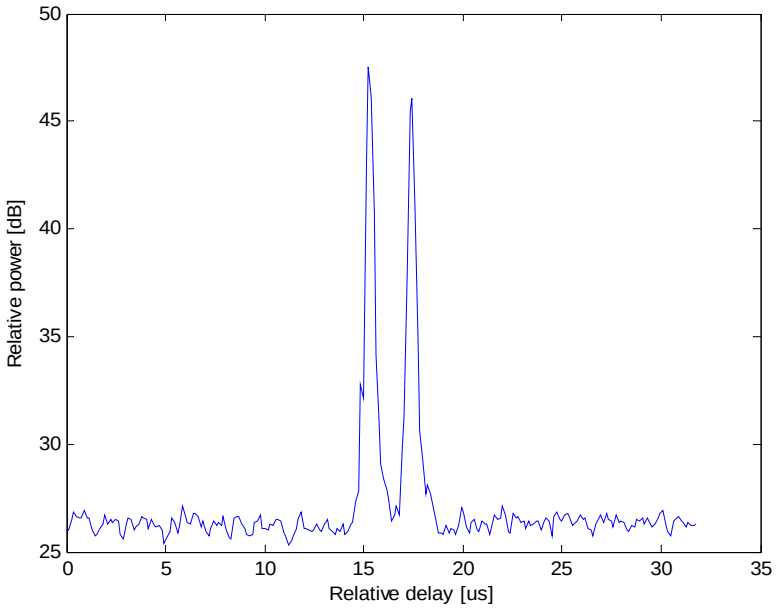

Figure 3-2: two-tap channel averaged power delay profile

The mean delay spread and rms delay spread computed for this channel model from (1) are $\mu_{Tm} = 1.07\mu s$ and $\sigma_{Tm} = 1.07\mu s$ respectively. It can be seen that for a two-tap channel both the mean delay spread and rms delay spread have the same value which is half of the delay difference between two taps.

We take average over the power delay profiles derived from the channel measurements to compare the result with the channel model in terms of the shape and rms delay spread. Figure 3-2 shows this mean power delay profile. The delay time between two taps of the power delay profile is about $2.08\mu s$ which is close to the delay time of the channel model ($2.14\mu s$).

The paths are expected to have almost the same power as the channel model represents. However, there is a power reduction of about 1.4 dB in the second tap. Both the power reduction and the delay difference are computed by considering all contributing points to the peaks.

The calculated rms delay spread for this power delay profile is $1.061\mu s$ which is again very close to that of the channel model $(1.07\mu s)$. On the other hand, the statistical rms delay spread of the power delay profiles can also be interesting to know. The median rms delay spread for this channel was $0.97\mu s$.

3.1.3 Channel A (2.72 km/h)

The other self-defined channel model is shown in the figure 3-3. In this model each tap is separated $0.5\mu s$ from the next one with a declining power of 3 dB. Taps in this model are separated enough to lead in resolvable paths in the impulse response of the channel. The vehicular speed was set to 2.72 km/h.

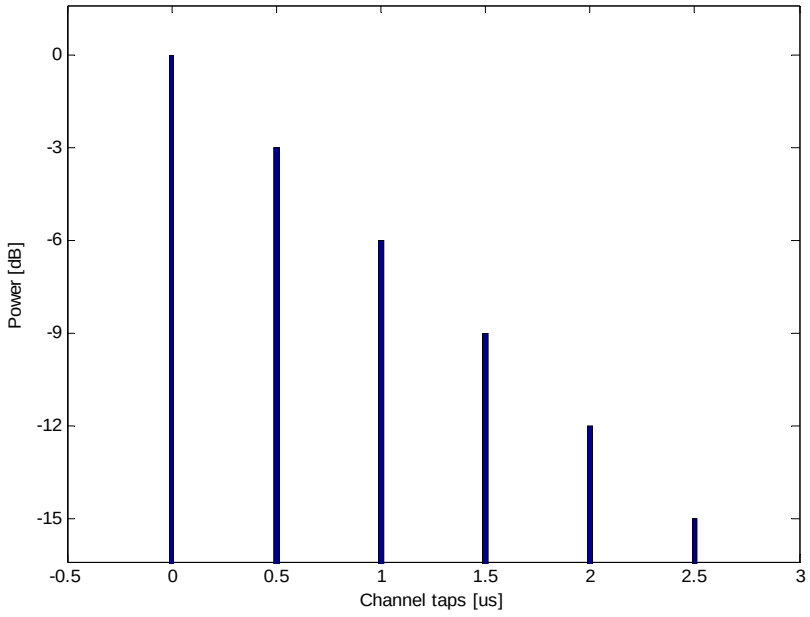

Figure 3-3: channel A

The calculated mean delay spread and rms delay spread of this channel are $\mu_{Tm} = 0.5165\mu s$ and $\sigma_{Tm} = 0.6296\mu s$ respectively. The averaged power delay profile obtained from the lab measurement is depicted in figure 3-4.

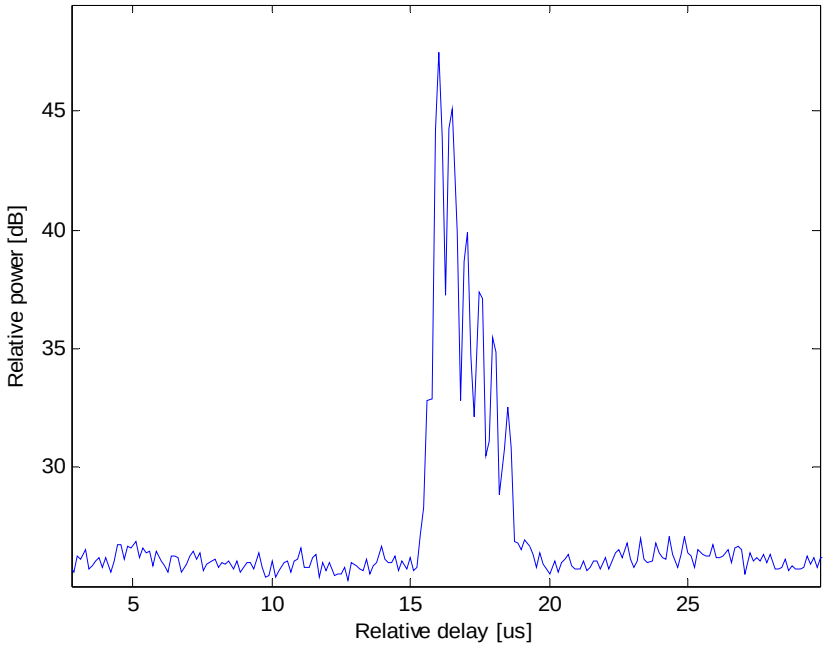

Figure 3-4: channel A averaged power delay profile

The shape of power delay profile almost represents the channel A model. But, in order to quantify this similarity, the delay time difference relative to the first tap as well as their power reductions are measured from the averaged power delay profile and tabulated in the following table. The table quantities are computed by considering all contributing samples to a peak.

Relative time	$0\mu s$	$0.52\mu s$	$1.04\mu s$	$1.5\mu s$	$1.96\mu s$	$2.48\mu s$
Relative power	$0dB$	$-2.9dB$	$-6.8dB$	$-9.8dB$	$-12.3dB$	$-14.3dB$

Table 3-1: channel A relative time/power

The power reduction is not consistently $-3dB$, however the delay times are almost around $0.5\mu s$. The fact that the delays are integer multipliers of the delay time $1/(2\times 3.84) = 0.13\mu s$, caused by half chip resolution, can make this deviation from the channel model.

The calculated rms delay spread of this power delay profile is $0.5975\mu s$ which can be compared to the channel model rms delay spread ($0.6296\mu s$). Statistically, the median rms delay spread of all measured power delay profiles is $0.5816\mu s$.

3.1.4 Channel A (100 km/h)

As the field measurement is performed with the normal driving speed. The channel estimates may also need to be evaluated in a rather high speed such as 100 km/h. Therefore, in another trial the channel emulator is set to the same channel A model but with the vehicular speed of 100 km/h. The averaged power delay profile is shown in figure 3-5.

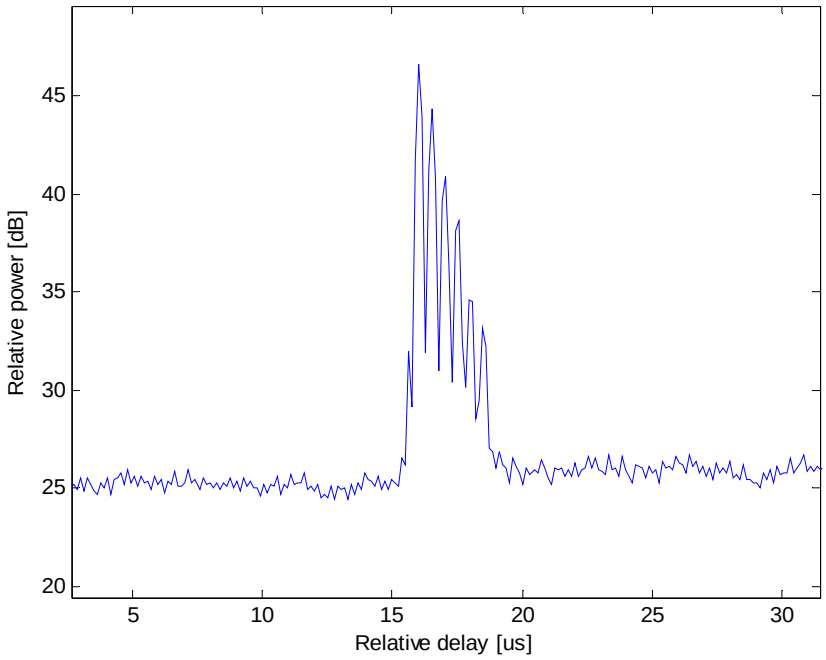

Figure 3-5: channel A averaged power delay profile in 100km/h

Again, the delay time difference relative to the first tap and the power value reduction are tabulated as the previous table.

Relative time	$0\mu s$	$0.52\mu s$	$0.98\mu s$	$1.44\mu s$	$1.96\mu s$	$2.47\mu s$
Relative power	$0dB$	$-2.5dB$	$-5.3dB$	$-7.5dB$	$-11dB$	$-12.7dB$

Table 3-2: channel A 100km/s relative time/power

The delay time is still around $0.5\mu s$, while the power reduction has more deviation from $-3dB$. The same explanation as mentioned above can be the reason for this difference to the model.

On the other hand, the computed rms delay spread of this power delay profile is $0.6229\mu s$ which is very close to that of the channel model ($0.6296\mu s$). By statistics, the median rms delay spread of all measured power delay profiles is $0.6381\mu s$ that is still close to rms delay spread of the channel model.

Due to the fact that WCDMA filter has a limited bandwidth and this bandwidth can cause the power delay profile paths not be resolvable, the channel estimation for the channels Ped A, TU and RA are evaluated only by the means of statistics.

3.1.5 Typical Urban channel (TU)

Generally, TU environment is referred to cities and towns where the buildings have nearly uniform height [2]. The TU channel we have worked with in the lab has 20 taps with a mobile speed of 3 km/h. The channel description is listed in the following table [4]. Relative times and powers in second and third columns are delay time and powers difference relative to the first tap.

Tap number	Relative time$[\mu s]$	Average relative power$[dB]$
1	0	-5.7
2	0.217	-7.6
3	0.512	-10.1
4	0.514	-10.2
5	0.517	-10.2
6	0.674	-11.5

7	0.882	-13.4
8	1.230	-16.3
9	1.287	-16.9
10	1.311	-17.1
11	1.349	-17.4
12	1.533	-19.0
13	1.535	-19.0
14	1.622	-19.8
15	1.818	-21.5
16	1.836	-21.6
17	1.884	-22.1
18	1.943	-22.6
19	2.048	-23.5
20	2.140	-24.3

Table 3-3: TU channel model description

The calculated mean delay spread and the rms delay spread for this channel are $\mu_{Tm} = 0.5195\mu s$ and $\sigma_{Tm} = 0.4915\mu s$ respectively.

On the other hand, the median rms delay spread of the all power delay profiles obtained from measurement is $0.4859\mu s$ which is very close to the rms delay spread of the channel model ($0.4915\mu s$).

3.1.6 Rural Area channel (RA)

The RA environment generally describes an environment with few buildings such as farmlands, fields and forests [2]. The RA channel set to the lab channel emulator is a channel with 10 delay taps and the relative times and power for each tap is listed as below [4].

Tap number	Relative time$[\mu s]$	Average relative power$[dB]$
1	0	-5.2
2	0.042	-6.4
3	0.101	-8.4
4	0.129	-9.3
5	0.149	-10.0
6	0.245	-13.1
7	0.312	-15.3
8	0.410	-18.5
9	0.469	-20.4
10	0.528	-22.4

Table 3-4: RA channel model description

The mean delay spread and the rms delay spread are calculated for this channel.

$\sigma_{Tm} = 0.1\mu s$

$\mu_{Tm} = 0.0885\mu s$

The median rms delay spread derived from the measured power delay profile is $0.1613\mu s$ which is not very close to rms delay spread of the channel ($0.1\mu s$). One reason can be that there is a lower boundary for the measured rms delay spreads of around $0.13\mu s$ caused by WCDMA half chip rate.

3.1.7 Pedestrian A channel

The pedestrian environment is characterized by small cells and low transmitting power. The BSes with low antenna heights are located outdoors; pedestrian users are located on street and inside buildings and residences [3]. The tapped-delay-line parameters of this channel are described in the following table [3].

Tap number	Relative time $[\mu s]$	Average relative power $[dB]$
1	0	0
2	0.110	-9.7
3	0.190	-19.2
4	0.410	-22.8

Table 3-5: Ped A channel model description

The calculated mean delay spread and the rms delay spread for this channel are $\mu_{Tm} = 0.0144\mu s$ and $\sigma_{Tm} = 0.046\mu s$ respectively.

The median rms delay spread derived from the measured power delay profile is $0.1329\mu s$ which is not again close to the channel model rms delay spread due to the same reasons. Table 3-6 summarizes all above measured rms delay spreads for different channel models.

Channel model	Theoretical	Empirical	
	Model rms delay spread [μs]	Avg. pdp rms delay spread [μs]	Median rms delay spread [μs]
Two-tap channel	1.07	1.06	0.97
Channel A(2.7km/h)	0.63	0.60	0.58
Channel A(100km/h)	0.63	0.62	0.63
TU channel	0.49	NA[4]	0.48
RA channel	0.10	NA	0.16
Ped A channel	0.05	NA	0.13

Table 3-6: summarizing table

[4] Not applicable as described in the text before.

As table shows, the theoretical results based on the channel models are very close to the empirical rms delay spreads derived from lab measurements for all channel models except the two last ones with very low rms delay spreads for which the WCDMA filter is the source of deviation. Hence, the measurements performed with our equipments result in accurate enough channel estimation. Consequently, we can conclude that the measurements are trustful to quite a large extent.

3.2 Initial Data Analysis

This section begins with data cleaning described in Pre-processing. Then, data classification is explained under the titles of Geographical coordinate assortment and Cell assortment. Initial data analysis will finish by data summarizing.

3.2.1 Pre-processing

As one of our measurement outputs is impulse response of the channel, one can compute rms delay spread of each instantaneous channel snapshot. However, not all channel snapshots are proper to be processed, as some are too weak in power or some are just noisy snapshots. Therefore, a first step to compute the rms delay spread is preprocessing the instantaneous power delay profiles which are obtained by parsing the measurement log files.

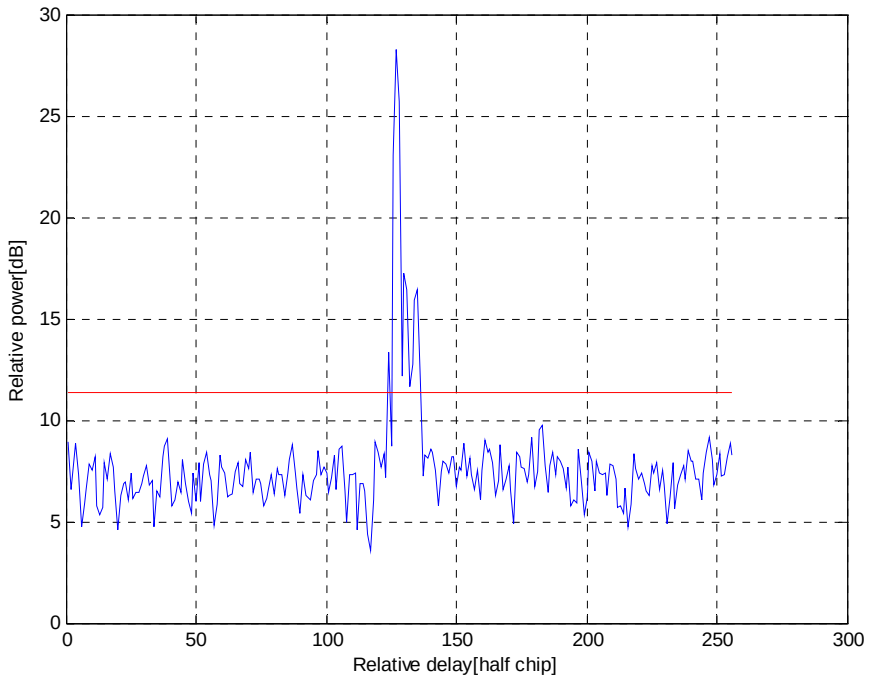

Figure 3-6: red line shows the noise level

Moreover, the rms delay spread is calculated only for instantaneous power delay profiles with a Signal-to-Noise Ratio (SNR) of higher than $12dB$. To compute the noise power, a noise level is assigned to each instantaneous power delay profile which is 4dB, decided by a rule of thumb, over the median of the profile. Additionally, the signal power, $P_{signal,dB}$, is calculated by summing the signal energy which is above noise level. The received power delay profile is shown by the blue signal in figure 3-6 and the noise level is shown by a red line.

However, it might be concerned that if any bias in rms delay spread values is introduced by applying this particular power threshold. This issue can be examined by a rms delay spread versus SNR plot as shown in figure 3-7. In this plot no noticeable trend in rms delay spread values is observed for different SNRes. Therefore, it seems that applying the described power threshold has not made any bias in rms delay spread values.

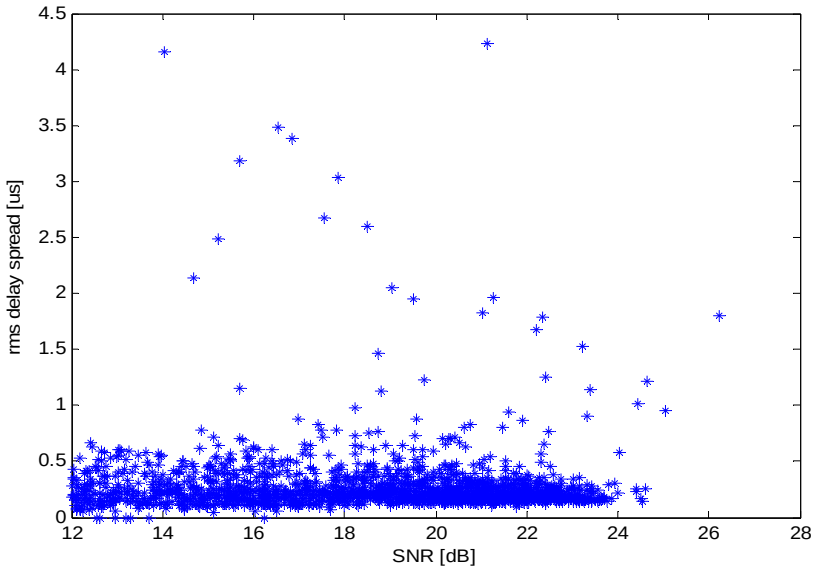

Figure 3-7: no bias is introduced by applying the described power threshold

3.2.2 Geographical coordinate assortment

The measurements are performed while driving a car with different speeds. On the other hand, the GPS device records information every second by second, while channel snapshots are recorded in milliseconds scale. Therefore, different number of channel snapshots is stored at each position depending on the movement speed. The faster movement results in less number of samples at each position and vice versa.

Considering the fact that the median of the rms delay spread is dependent on the number of samples at each geographical point, we should try to smooth the data. In other words, we should have almost constant number of samples for each coordinate. Hence, one primary task is to map the power delay profile samples and RRC measurement reports to their relative geographical points and aggregate all rms delay spreads and RSCPes corresponding to one single coordinate.

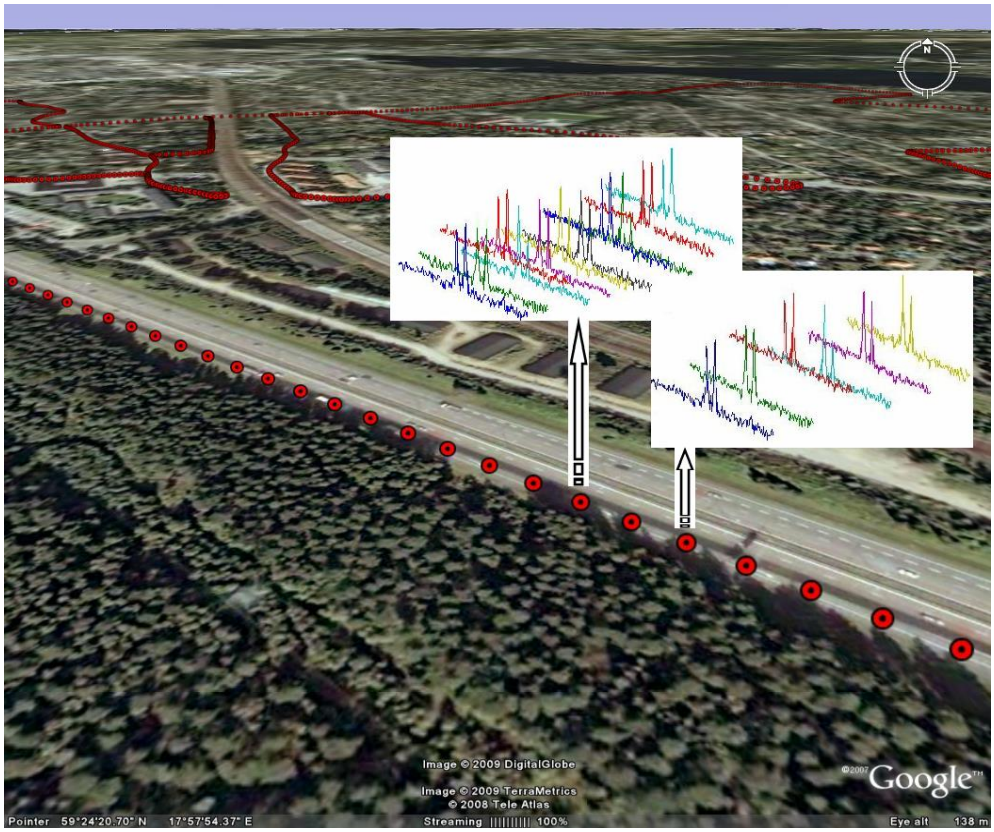

Figure 3-6: geographical coordinate assortment

- *Mapping power delay profiles to GPS coordinates*

As mentioned before, every GPS coordinate is tagged with its recording time synchronized with GMT, and on the other hand every power delay profile is also marked with a time-stamp. Therefore, the power delay profile samples and consequently their relative rms delay spreads can be mapped to their corresponding GPS coordinate by easily comparing the GPS time and log time-stamps. We should recall that log time-stamp is not synchronized with GPS time. So, one of them should be converted to the other one.

- *Mapping RRC measurement report to GPS coordinates*

Since the RRC measurement report records RSCP values from all receiving cells, they may also be classified based on their recorded coordinates. The procedure is the same as mapping power delay profiles to GPS coordinates. The time-stamps for RRC measurement report should be extracted separately while parsing the log file so that they can be compared to GPS time in order to sort the relative RSCP values of each GPS coordinate.

It also should be noted that while GPS time is increasing, the GPS coordinates may appear still, i.e. the car is still. So, the power delay profile samples or RRC measurement reports of these identical GPS coordinate should be all aggregated and put in one group assigned to the considered GPS coordinate.

3.2.3 Cell assortment

Although rms delay spreads and RSCP values are classified based on their geographical position, still they come from different receiving cells. Thus, rms delay spreads and RSCPes at one specific coordinate should be sorted and grouped based on their corresponding SCes.

As SCes for both power delay profiles and RRC measurement reports are recorded and extracted in previous stages, we know the SC corresponding to each rms delay spread or to each RSCP. Thus, we can easily find the identical SC received at each coordinate and group their corresponding rms delay spread or RSCP values.

Now, for each coordinate there are groups of rms delay spreads and groups of RSCPes. To summarize the data, we use median to get a single value for each group of rms delay spread or RSCP. The cell assortment procedure and data summarizing are more described both for rms delay spreads and for RSCPes in the figures below for one coordinate.

$$\left[latitude_1\ longitude_1\right] \Rightarrow \begin{bmatrix} \sigma_{Tm,1} \\ \sigma_{Tm,2} \\ \sigma_{Tm,3} \\ \sigma_{Tm,4} \\ \sigma_{Tm,5} \\ \vdots \\ \sigma_{Tm,n} \end{bmatrix} \sim \begin{bmatrix} sc'_1 \\ sc'_2 \\ sc'_1 \\ sc'_3 \\ sc'_3 \\ \vdots \\ sc'_n \end{bmatrix} \Rightarrow \begin{bmatrix} median(\sigma_{Tm,1}, \sigma_{Tm,3}, \cdots) \\ median(\sigma_{Tm,2}, \cdots) \\ median(\sigma_{Tm,4}, \sigma_{Tm,5}, \cdots) \\ \vdots \\ median(\cdots, \sigma_{Tm,n}) \end{bmatrix} \sim \begin{bmatrix} sc'_1 \\ sc'_2 \\ sc'_3 \\ \vdots \\ sc'_n \end{bmatrix}$$

Figure 3-7: Cell classification for rms delay spreads

$$\left[latitude_1\ longitude_1\right] \Rightarrow \begin{bmatrix} RSCP_1 \\ RSCP_2 \\ RSCP_3 \\ RSCP_4 \\ RSCP_5 \\ \vdots \\ RSCP_m \end{bmatrix} \sim \begin{bmatrix} sc''_1 \\ sc''_2 \\ sc''_3 \\ sc''_3 \\ sc''_1 \\ \vdots \\ sc''_m \end{bmatrix} \Rightarrow \begin{bmatrix} median(RSCP_1, RSCP_5, \cdots) \\ median(RSCP_2, \cdots) \\ median(RSCP_3, RSCP_4, \cdots) \\ \vdots \\ median(\cdots, RSCP_m) \end{bmatrix} \sim \begin{bmatrix} sc''_1 \\ sc''_2 \\ sc''_3 \\ \vdots \\ sc''_n \end{bmatrix}$$

Figure 3-8: Cell classification for RSCPes

However, we should note that the number of SCes for RSCP might be different from the number of that for rms delay spread, because RSCP and rms delay spread are derived from two different types of records and in some cases the impulse response of one BS is not recorded, while RRC measurement reports its corresponding RSCP value. Hence, in order to relate the rms delay spread and RSCP, only the values are picked which have SCes in common. Thus:

$$\left[latitude_1\ longitude_1\right] \Rightarrow SC = (SC_{\sigma_{Tm}} \cap SC_{RSCP}) \Rightarrow \begin{bmatrix} sc_1 \\ sc_2 \\ sc_3 \\ \vdots \\ sc_k \end{bmatrix} \sim \begin{bmatrix} \sigma_{Tm,1} \\ \sigma_{Tm,2} \\ \sigma_{Tm,3} \\ \vdots \\ \sigma_{Tm,k} \end{bmatrix} \sim \begin{bmatrix} RSCP_1 \\ RSCP_2 \\ RSCP_3 \\ \vdots \\ RSCP_k \end{bmatrix}$$

Figure 3-9: Finding the joint SCes

One question which can be arisen here is how much the whole processing over the raw data statistically affects the derived parameters. To answer this question, the rms delay spread values of one of measurement campaigns in Stockholm are computed before any classification and they are compared with the rms delay spread values from the processed data of the same source. Figure 3-10 shows the CDF distribution of these two data sets and as it is clear they are very close to each other. This can indicate that processing the data does not affect the rms delay spread statistics.

3.3 Analysis results

The classified and summarized data can now be analyzed. The rms delay spread of impulse responses includes the main interesting part of the analyzed data. Figures 3-11, 3-12, 3-13 demonstrate three examples of impulse responses with low, medium and high rms delay spread respectively.

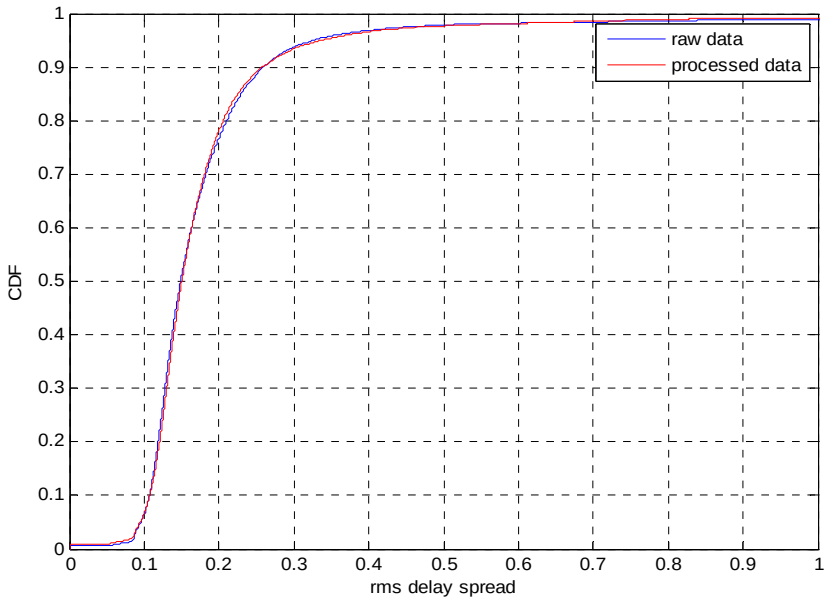

Figure 3-10: rms delay spreads from raw data and processed data are compared

The first sub-section describes the rms delay spread distribution of different areas with a comparison to current channel models. The next sub-section, 3.3.2, compares the analysis result with some currently used channel models. Sub-section 3.3.3 describes how forest can affect on the delay spread in rural areas. The next sub-sections of 3.3.4 to 3.3.6 present the relationships between rms delay spread, base-mobile distance and RSCP to figure out any correlation. Finally, the correlation of delay spreads within and between sites is discussed in the last sub-section.

Moreover, the color coded GE files are used along the work as descriptive tools. In section 2.4.1, these GE files have been described for any general numerical value. Here, we use this feature of GE to better illustrate the rms delay spread and RSCP values in the measured routes.

These color coded paths help to see how rms delay spread or RSCP changes throughout the routes, how different environments can affect them and how getting close to or far from the BSes can be effective on both the rms delay spread and RSCP values.

The GE files were written in a way that one can see all the data points corresponding to each single BS. Therefore, all data sets of each SC including rms delay spreads, RSCPes, their GPS coordinates and the GPS coordinate of the corresponding BS were organized in one group before plotting the color coded paths.

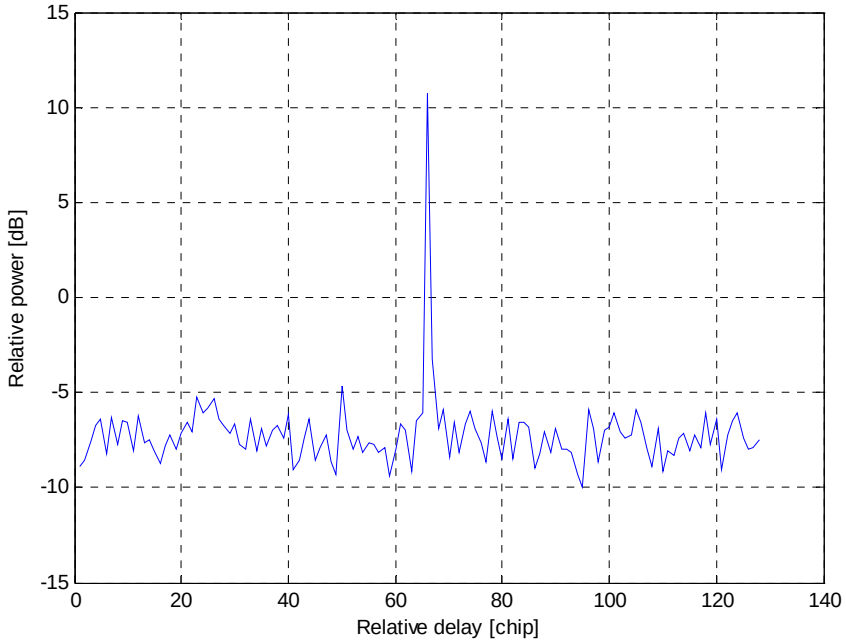

Figure 3-11: impulse response with low rms delay spread about $0.05\,\mu s$

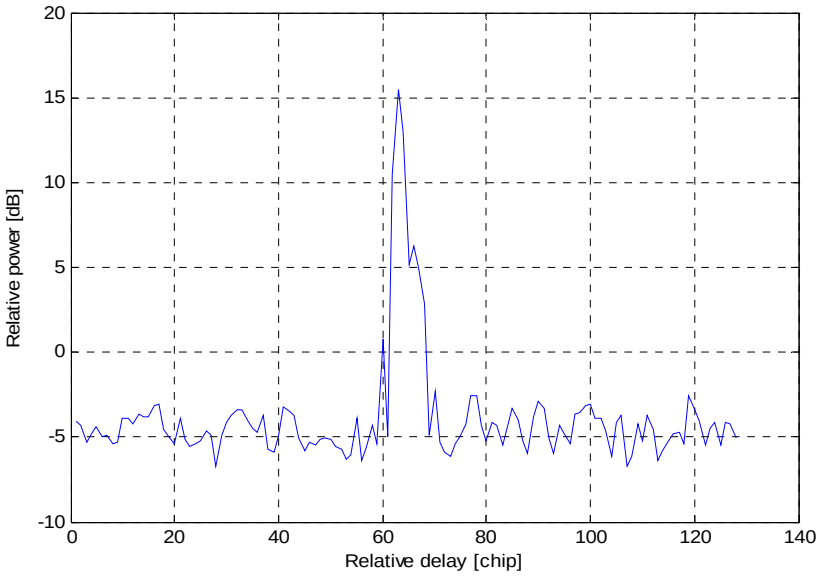

Figure 3-12: impulse response with medium rms delay spread about $0.19\,\mu s$

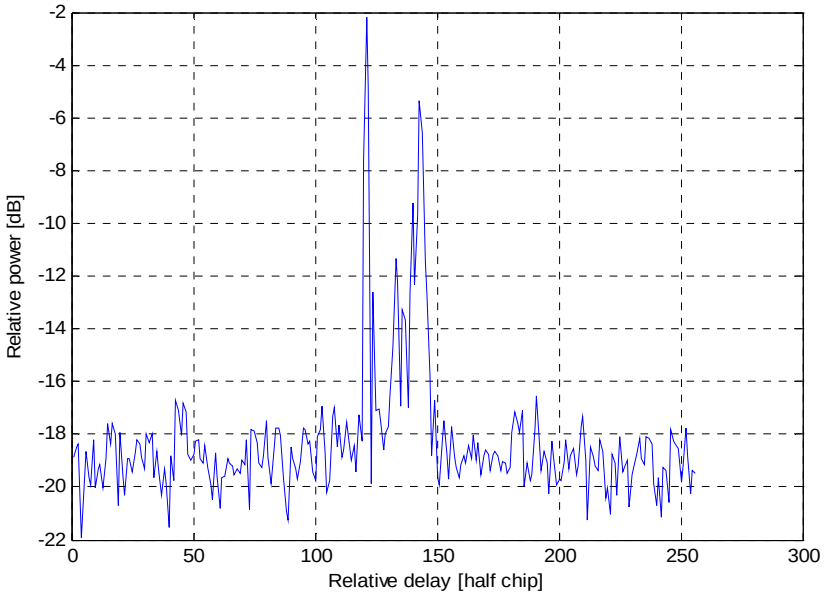

Figure 3-13: impulse response with high delay spread about $1.3\mu s$

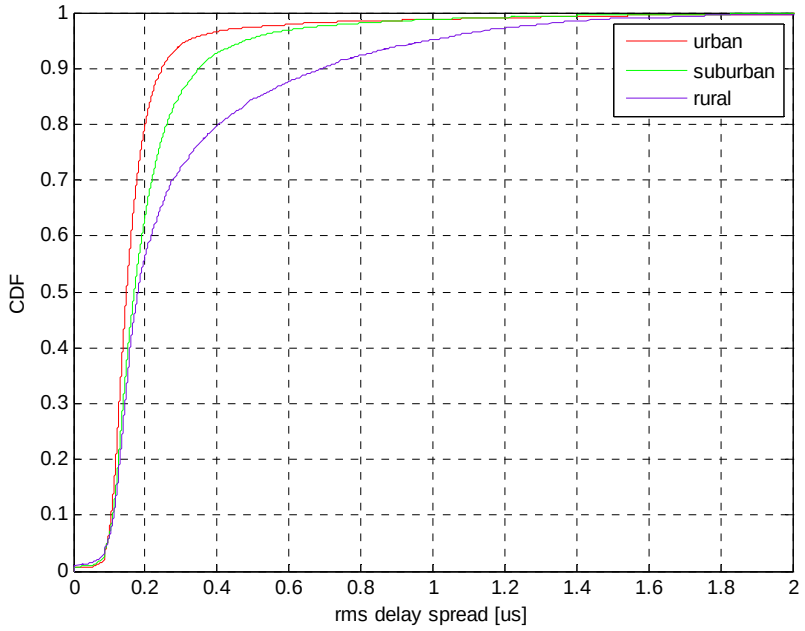

Figure 3-14: rms delay spread distribution of Stockholm for urban, suburban and rural

3.3.1 The distribution of the rms delay spread

The rms delay spread values can be described statistically by their distribution function. Also, their distribution can be quantified by the median value. In continue the rms delay spread distributions of variant environmental types are illustrated and compared.

Stockholm: as described before, three environmental types of urban, suburban and rural have been covered in the Stockholm measurements. The distribution functions of all three environments are compared in figure 3-14.

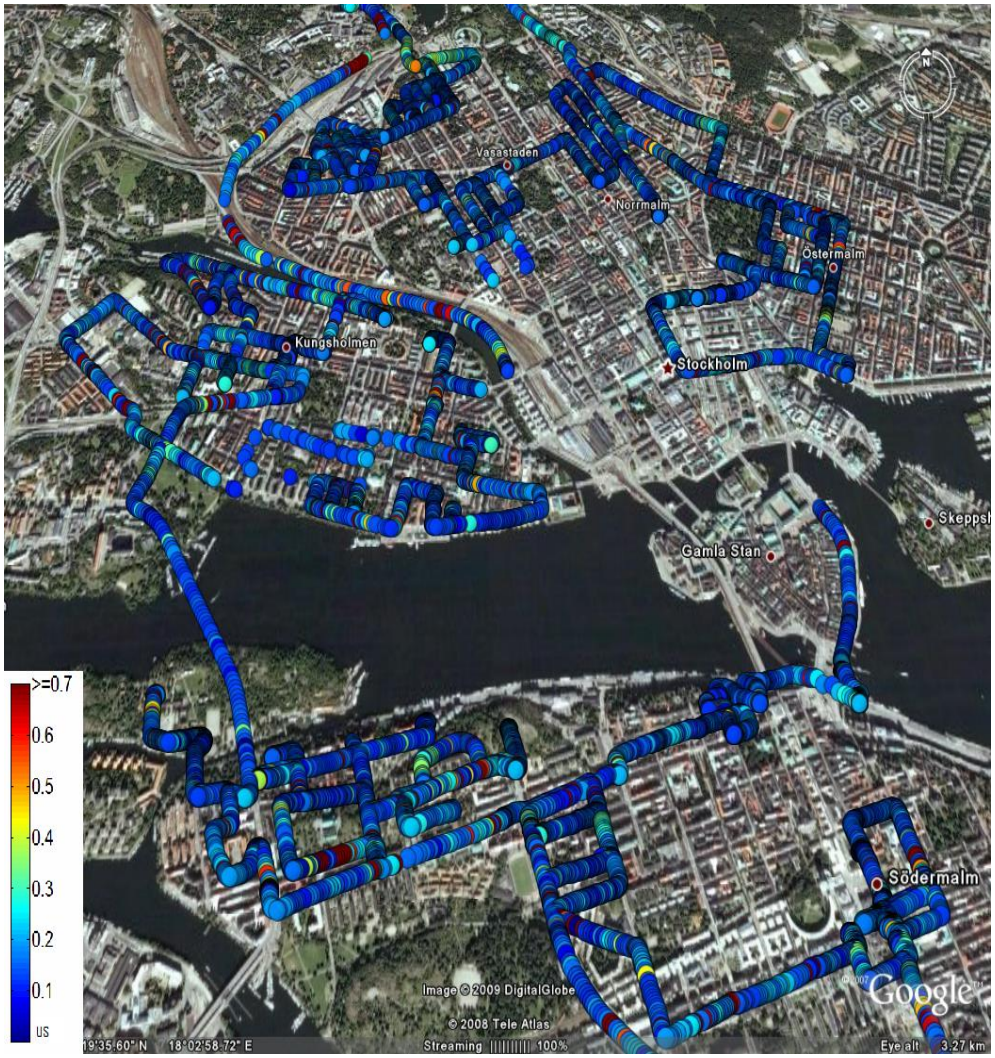

Figure 3-15: rms delay spread in an urban area GE snapshot, map size: 5×6*km*

As seen in the figure, rural area shows the highest and the urban area shows the least values of rms delay spread in Stockholm as it is evidenced in color coded GE images representing rms delay spread values. There are more spots with higher values (red color dots) in the rural area than in urban area. Figures 3-15 and 3-16 are two snapshots of rural and urban areas demonstrating the rms delay spread values.

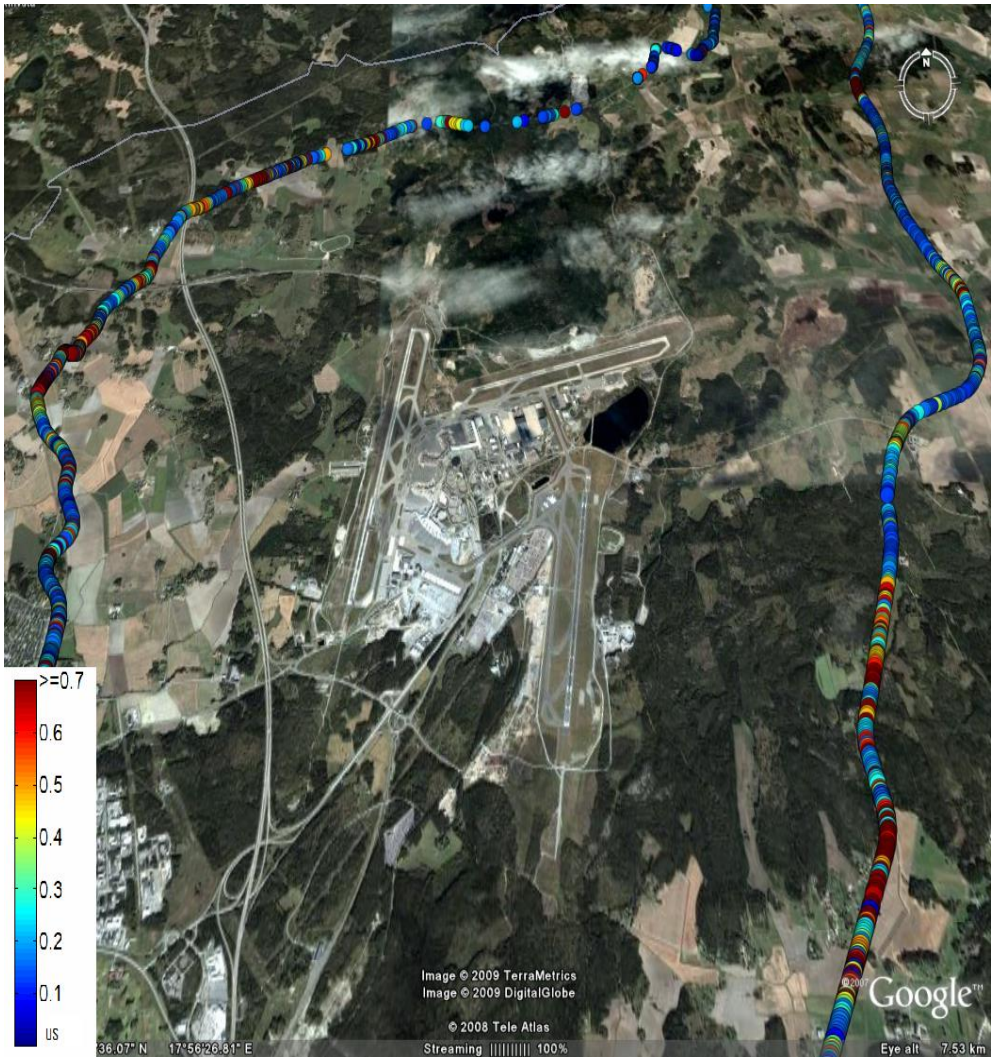

Figure 3-16: rms delay spread in a rural area GE snapshot, map size: $12 \times 15 km$

The fact that the downtown area in Stockholm has a homogeneous structure with medium-height buildings in combination with small cell sizes can lead to direct paths and near-distance scattering or reflections. This can result in channel impulse

responses with single ray clusters. On the other hand, interfering objects in suburban and rural areas are more apart from each other which can cause distant reflections appearing as multi clusters in impulse responses.

Furthermore, the scattering from forest edges can also be considered as a hypothesis to cause high rms delay spread in some rural vegetated areas. This hypothesis is more discussed in 3.3.4.

Considering the fact that there are large areas of water in Stockholm downtown, can arise the question that what is water effect on rms delay spread. According to another measurement results also investigated in Stockholm downtown [15], more scattering has been observed in the vicinity of water. This measurement has been taken by one single BS and one mobile station. In our case, however there has not been any noticeable difference between paths close to or far from the water.

Atlanta: the distribution of rms delay spreads for urban, suburban and highways in Atlanta are compared in the figure below.

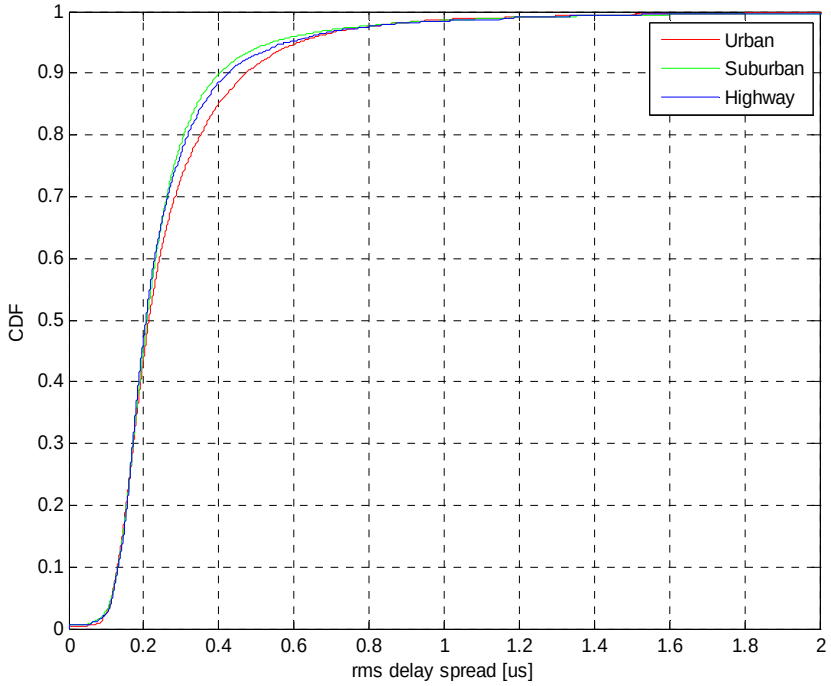

Figure 3-17: rms delay spread distribution of Atlanta
for urban, suburban and highway

In Atlanta, rms delay spread values are quite close in suburban and highway, as highway is indeed a part of suburban area. On the other hand, urban shows slightly higher values of rms delay spread which can be due the fact that downtown area of

Atlanta has a heterogeneous structure with high-rise buildings causing higher rms delay spreads [9], While suburban of Atlanta has a smoother structure and can lead to lower delay spread. In the figure below, one sample snapshot of Atlanta rms delay spread is shown.

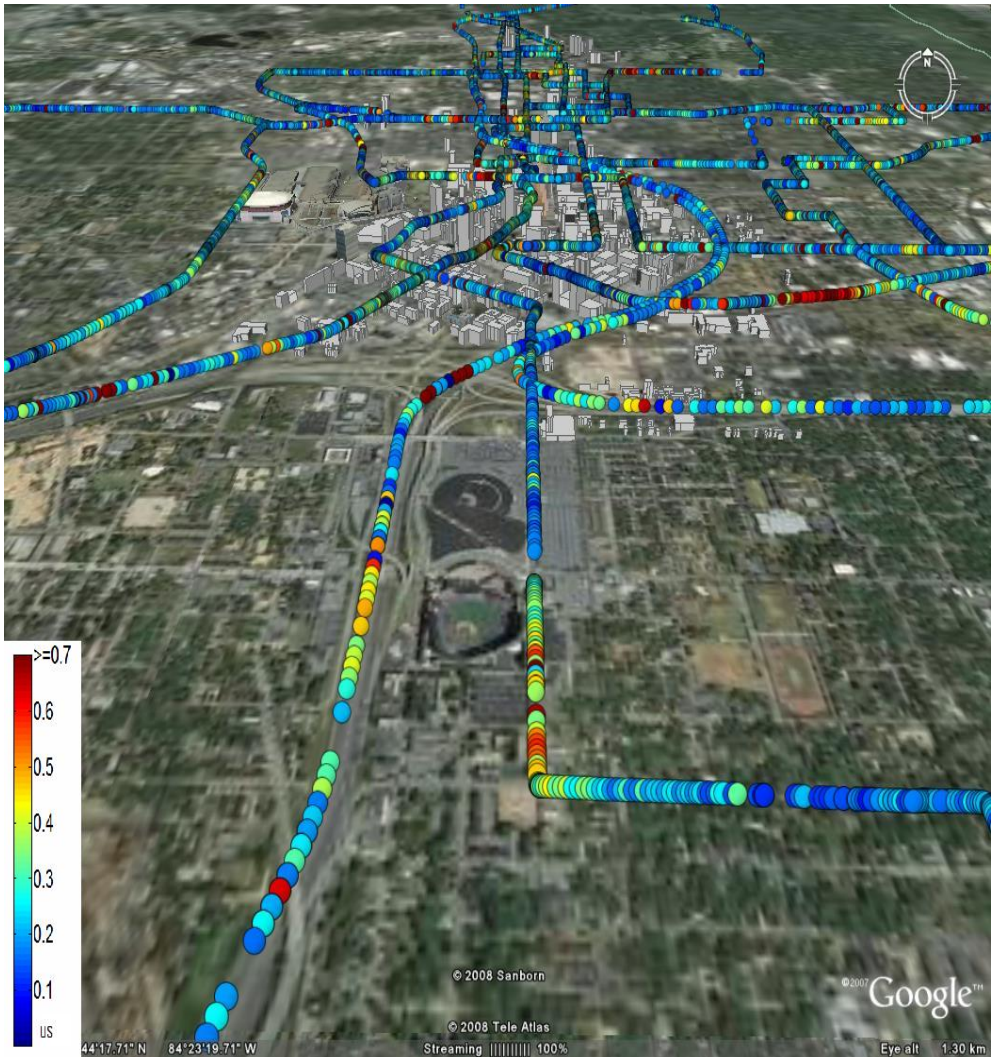

Figure 3-18: rms delay spread in a GE snapshot in Atlanta, map size: $3 \times 7 km$

Stockholm and Atlanta (urban, suburban): it might be also interesting to see how the rms delay spread differs for two cities with different structures. So, the distribution functions of them for urban and suburban areas are compared in the following plot.

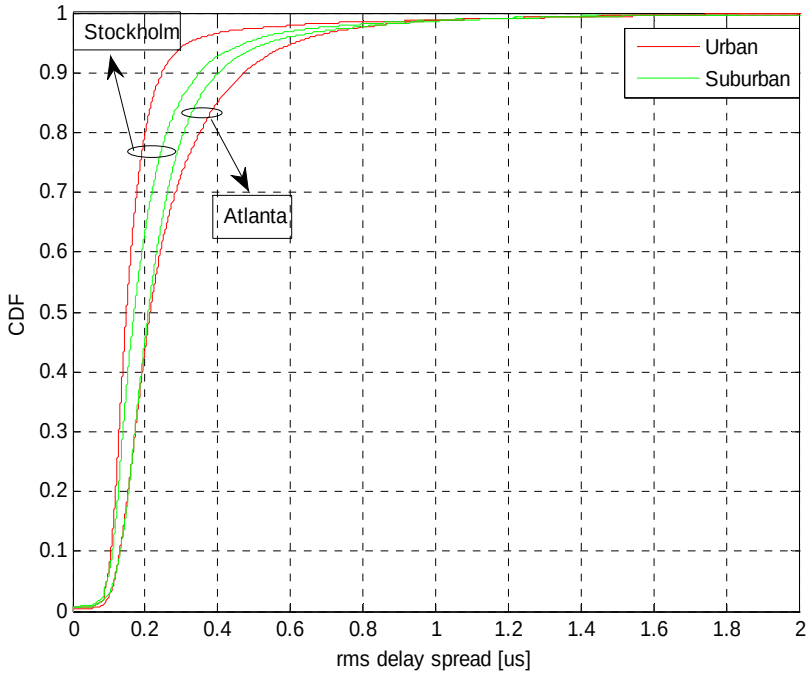

Figure 3-19: Comparing rms delay spread distribution of Stockholm and Atlanta

As figure shows, both urban and suburban in Atlanta introduce higher rms delay spread values than Stockholm. Moreover, in Atlanta the rms delay spreads for urban is slightly higher than suburban and highway which is in contrast with Stockholm. One reason can be that the European city structure of Stockholm in comparison with American city style of Atlanta has a milder interfering structure causing lower rms delay spreads.

This structure difference is more obvious in the urban areas of these cities which can also be seen in the red curves of above figure which are more diverse from each other than the green curves representing the suburban areas. The suburban structures of these cities are similar which lead to similar rms delay spread distribution.

France: two environmental types of urban and highway are covered in France, Urban area of Lille, a city in France, and some highways around it. The measurement data of each is processed separately in the same way done for Stockholm and Atlanta. The rms delay spread distributions of each area is depicted in the figure 3-20.

The curves are very close to each other. Only the tale of the curves shows a slightly higher rms delay spread for highway. Figure 3-22 demonstrates one example of rms delay spread values demonstrated in GE in Lille.

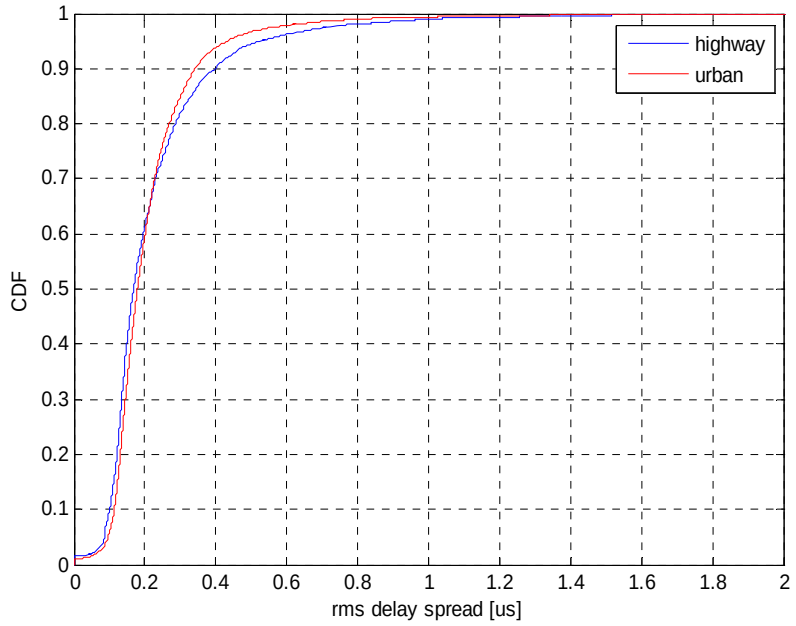

Figure 3-20: rms delay spread of France for urban and highway

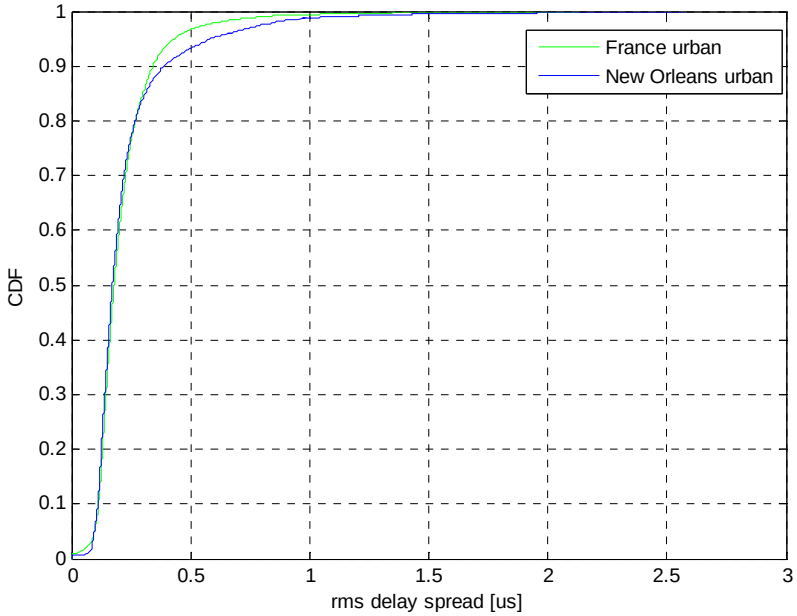

Figure 3-21: comparing rms delay spread distributions of France and New Orleans in urban area

France and New Orleans: the distribution of rms delay spread for both France and New Orleans in urban area can also be plotted and compared versus each other. Figure 3-21 depicts such a plot.

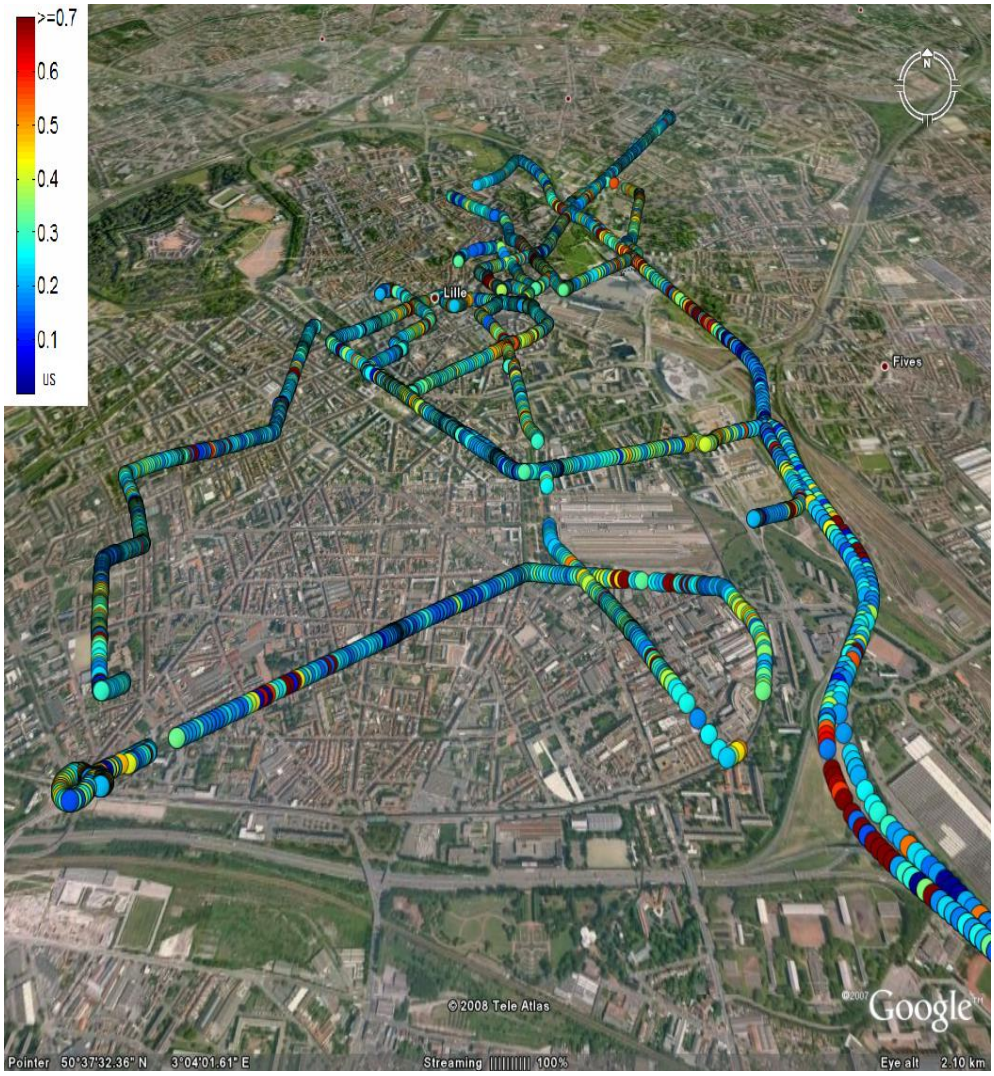

Figure 3-22: rms delay spread in a GE snapshot in Lille, map size: $4 \times 7 km$

The rms delay spread distributions of these two areas are very similar to each other. As mentioned before, measurements in New Orleans were performed in the French

Quarter area with old European style. Hence, the comparable structure of these two cities can describe their similarity of delay spread.

In order to quantify and summarize the statistical characterization of the rms delay spreads for all areas discussed above, the medians as well as 90th-percentile of rms delay spreads are tabulated.

City	Covered areas	Median of rms delay spread [μs]	90th-percentile of rms delay spread [μs]
Stockholm	Urban	0.15	0.25
	Suburban	0.17	0.37
	Rural	0.18	0.69
Atlanta	Urban	0.21	0.47
	Suburban	0.21	0.40
	Highways	0.21	0.43
France	Urban	0.18	0.34
	Highways	0.17	0.40
New Orleans	Urban	0.17	0.39
All measurements		0.18	0.38

Table 3-7: median of rms delay spreads

The 90th–percentile of rms delay spread highlights the delay spread variation of different areas, particularly, the urban, suburban and rural area of Stockholm. Also, the last row of the table shows the average of median and 90th-percentile rms delay spread values of all measurements.

3.3.2 Results comparison with channel models

One of the thesis goals is to compare the measurement results with current channel models. Hence, the distributions of these channel models can be considered and plotted in the same figures as above for different areas. Here is a list of considered models for comparison:

- *3GPP TU and RA [4], GSM TU and RA [11], Pedestrian A and B [3], Vehicular A and B [3], SCM Urban and Suburban [12].*

In the figure 3-23, the distribution of rms delay spread in Stockholm is compared with 3GPP TU and RA, GSM TU and RA and also with SCM Urban and Suburban. As it can be seen, 3GPP RA and GSM RA have very similar distribution and both show smaller rms delay spreads than our measurement results in rural area (purple curve). On the other hand, our measurements results in urban area of Stockholm demonstrate much lower rms delay spread than both 3GPP TU and GSM TU. Similar results have been noticed in [13]. Considering SCM models, SCM suburban is well matched with our data, while SCM urban shows higher rms delay spreads.

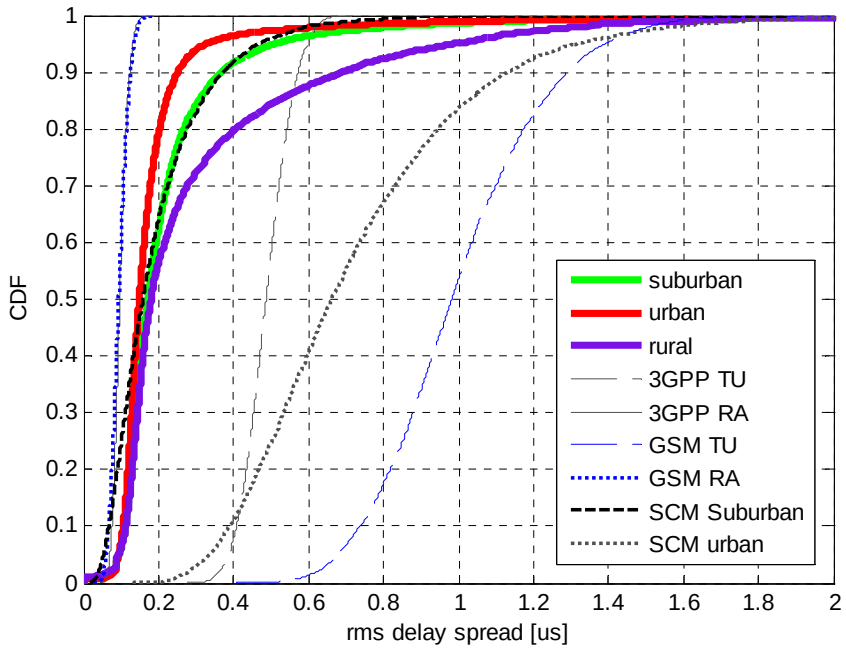

3-23: Stockholm distribution against some current channel models

Table 3-8 summarizes the median rms delay spread of all above channel models as well as Ped A, B and Veh A, B to make the comparison with the measurement data.

Channel Model	Median rms delay spread [μs]
Pedestrian A	0.045
Pedestrian B	0.75

Vehicular A	0.37
Vehicular B	4
3GPP TU	0.49
3GPP RA	0.10
GSM TU	0.98
GSM RA	0.94
SCM suburban	0.16
SCM urban	0.65

Table 3-8: Median rms delay spread for Ped A, B and Veh A, B

From table 3-7 and 3-8, it is obvious that all the channels above have distinctly higher median rms delay spread except for Pedestrian A which has lower delay spread. A similar figure can be plotted for Atlanta as figure 3-24 shows.

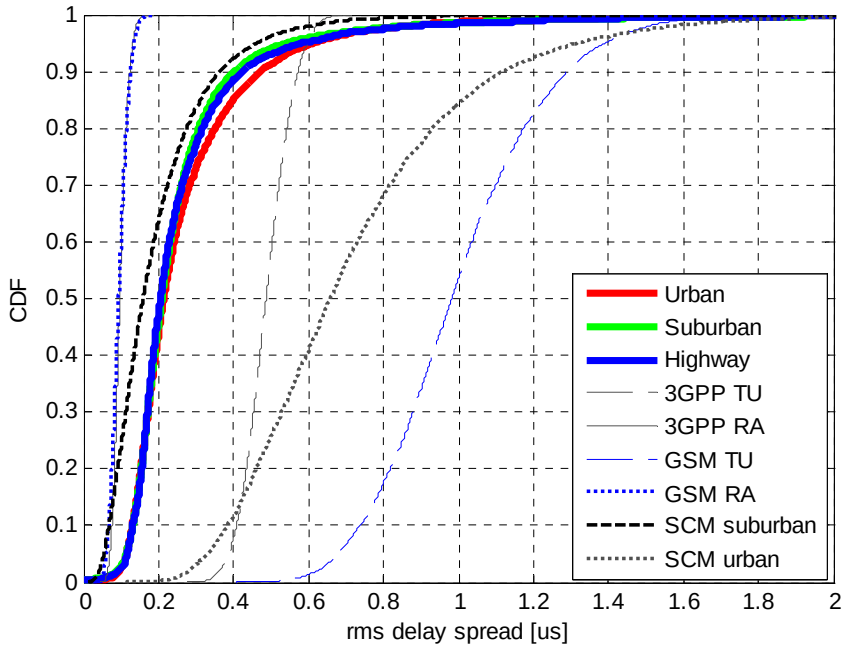

Figure 3-24: Atlanta distribution against some current channel models

Still, SCM Suburban fits well to our data, while the other channel models as 3GPP TU, GSM TU and SCM urban demonstrate higher rms delay spreads and 3GPP RA and GSM RA demonstrate lower ones. In case of Pedestrian and Vehicular channel models, the same conclusion as Stockholm holds.

3.3.3 Forest effect on delay spread

As higher rms delay spread has been observed in vegetated rural areas, it brings up this hypothesis that forest edges may cause large rms delay spread. Therefore, some different cases were examined to test this effect. Here is one of these examined examples. The figure 3-26 shows 4 possible paths for the 4 taps of the corresponding power delay profile, shown in figure 3-25, obtained for one specific examined point (point C). The rms delay spread for this power delay profile is about $0.7\mu s$. Also, this power delay profile is calibrated based on its relative RSCP value to have the power values in the right and true scale; i.e. the initial delay profile is normalized and then multiplied with the RSCP value.

The paths shown in GE image correspond quite well to the power delay profile taps. The path1 or LOS is considered as the reference path and it corresponds to the first tap. The delay time between the first tap and second tap is $0.4\mu s$. This delay time fits to the path length difference of path1 and path2 which is about $125m$. Similarly, the difference between length of path3 and path1 is about $275m$ which may correspond to the tap3 and tap1 delay time difference of $0.9\mu s$. At last, the delay time and path length difference for tap 4 is $1.4\mu s$ and $425m$ respectively.

We can also examine the scattered power from the forests to check if it has the same order of magnitude as received power indicated in power delay profile or not. Among the paths, path3 and path4 are considered as possible paths for rays scattered from the forests as shown in the GE image. We chose path3 to examine its scattered power. From bistatic radar equation [16]:

$$Pr_C = Pt_A G_C G_A \left(\frac{\lambda}{R_1 R_2}\right)^2 \frac{1}{(4\pi)^3}\sigma \qquad (2)$$

Where Pr_C is the received scattered power at point C, Pt_A is the transmitted power by antenna at point A, G_A and G_C are antenna gains, R_1 and R_2 are shown in the figure and σ is the scattering cross section. If we consider a scattering plane in side B consisting of N trees, we can say Pr_C is the power indicated in tap3 of power delay profile divided by N. In our case the plane length is about 200m and by considering 1m-radius-trees, we estimate N=100. Hence:

$$Pr_C = \frac{P_{tap3}}{N} = \frac{8.5\times10^{-15}}{100} W \qquad (3)$$

On the other hand, Pt_A, the transmitted power of BS can be extracted from the relative operator site information which states a value about $30dBm$ or $1W$ in linear scale as the average transmitted power of the BSes. The antenna gain at BS, G_A, is typically between $14-18dBi$ or $25-60$ in linear scale. Thus, as estimation we can consider G_A about 50. Also, G_C the antenna gain at the terminal is typically about $-10dBi$. However, it is appropriate to consider an additional $10dB$ penetration loss as the terminal is inside the car. Hence, $-20dBi$ or 0.01 seems reasonable for G_C. Therefore, with substituting all parameters:

$$\frac{8.5\times10^{-15}}{100}=1\times50\times0.01\times(\frac{3\times10^{8}/1.9\times10^{9}}{800\times500})\times\frac{1}{(4\pi)^3}\times\sigma\xrightarrow{Yields}\sigma\simeq2.2m^2\simeq3.4dBm^2 \quad (4)$$

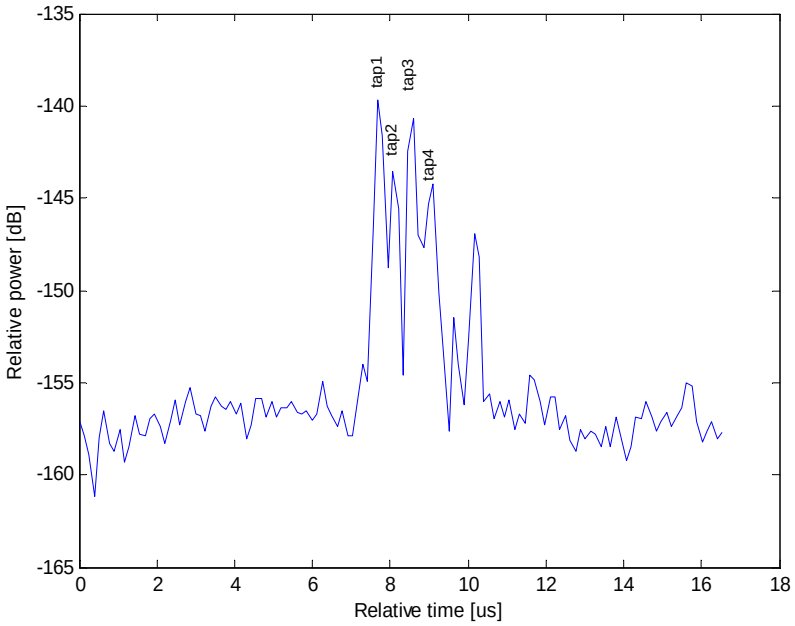

Figure 3-25: power delay profile obtained in point C

This σ introduces the scattering cross section of one tree. [14] presents a model for the scattering of radio waves of one single tree. Figure 5 in [14] shows the theoretical scattering cross sections of a tree at $1.9GHz$ for a 1m-radius-tree. The resulted σ in our case is in the range of this figure curve which falls in an approximate interval of $0-5dBm^2$ for scattering degrees of $45^\circ-180^\circ$. Examining other cases in rural area

resulted in similar scattering cross section values. However, we should note that we can never identify the true scatterers with any certainty. Hence, any conclusion must be regarded as tentative.

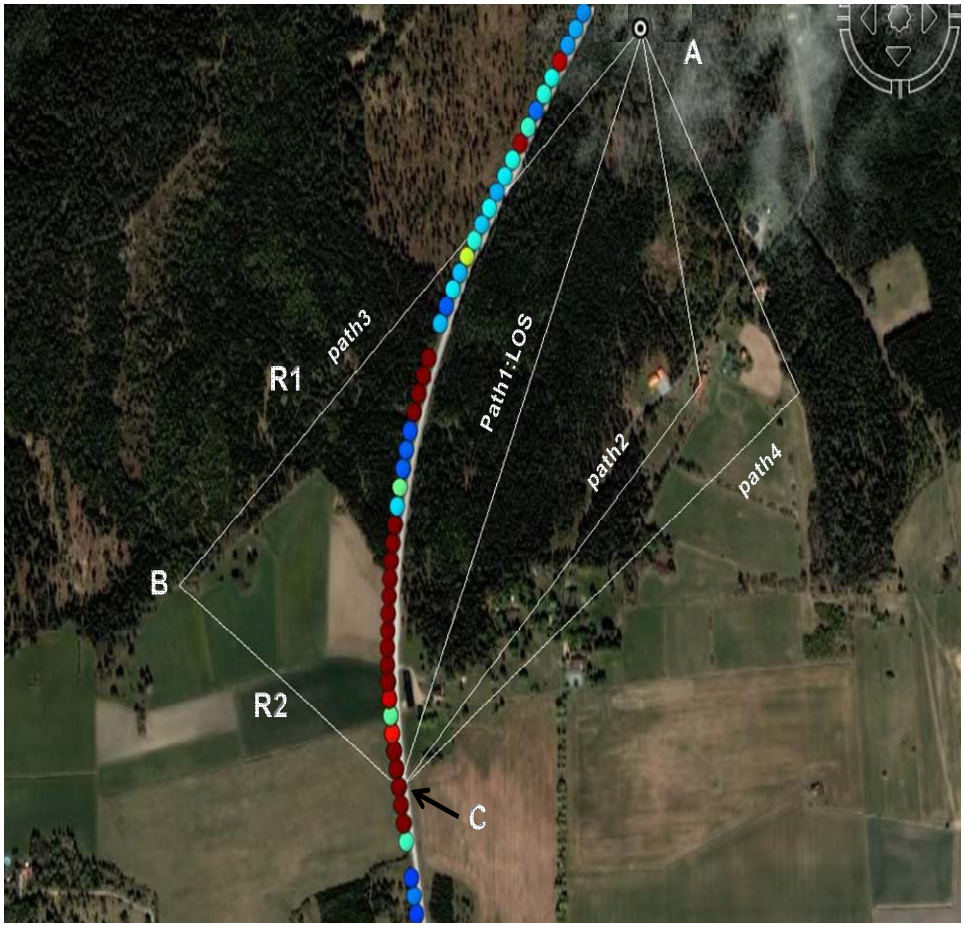

Figure 3-26: Four possible paths relative to power delay profile at point C

3.3.4 rms delay spread versus base-mobile distance

The cell site information, one very useful piece of information, provided by both the operators in Stockholm and Atlanta enabled us to find the instantaneous base-mobile distance at each point. The cells GPS coordinates and cells SCes were extracted from the site information.

As we already knew the SCes, the rms delay spreads and the RSCPes at each geographical coordinate from (*3.2.3*), we can find and assign the corresponding cell location of each rms delay spread and RSCP. We should only note that the cells are

reused in the network and trying to find the match location of each SC can result in two or three locations. However, the correct cell location is the closest one to the mobile position. Hence, we pick the location with the minimum base-mobile distance. Therefore, the following data are obtained for one mobile position of [*latitude1 longitude1*].

$$\left[latitude_1\ longitude_1 \right] \Rightarrow \begin{bmatrix} sc_1 \\ sc_2 \\ sc_3 \\ \vdots \\ sc_k \end{bmatrix} \sim \begin{bmatrix} lat_{sc1} lon_{sc1} \\ lat_{sc2} lon_{sc2} \\ lat_{sc3} lon_{sc3} \\ \vdots \\ lat_{sck} lon_{sck} \end{bmatrix} \sim \begin{bmatrix} dis_1 \\ dis_2 \\ dis_3 \\ \vdots \\ dis_k \end{bmatrix} \sim \begin{bmatrix} \sigma_{Tm,1} \\ \sigma_{Tm,2} \\ \sigma_{Tm,3} \\ \vdots \\ \sigma_{Tm,k} \end{bmatrix} \sim \begin{bmatrix} RSCP_1 \\ RSCP_2 \\ RSCP_3 \\ \vdots \\ RSCP_k \end{bmatrix}$$

Figure 3-27: obtained data at each GPS coordinate of mobile terminal

In order to compute the distance between two points of [*lat1 lon1*] and [*lat2 lon2*], the great circle formula was used which is defined as:

$$dis = arc\cos(\sin(lat1)\cdot\sin(lat2) + \cos(lat1)\cdot\cos(lat2)\cdot\cos(lon1 - lon2))\cdot R\_earth \qquad (5)$$

Where R_earth is the radius of the earth equal to $6371km$. Now, having the data sets of rms delay spreads and their corresponding base-mobile distances can help to figure out how rms delay spread might change with base- mobile distance or if there is any correlation between them or not. Plotting these two data sets can illustrate any trend of rms delay spread versus distance. However, finding this relationship can be tricky by using their scattering plot as there are fewer data points for longer distances. Another method is to group the data sets so that all elements within a specific distance interval (x meter) will be summarized by their median. Then, the new data sets consisting of median rms delay spreads and their relative distances can be plotted.

The following plots depict the rms delay spread versus base-mobile distance relationship in Stockholm and Atlanta respectively. The figures are plotted for $x = 20m$. The histogram of the data is also shown to know how many data points are used for each distance interval.

Moreover, comparing the histograms of Stockholm and Atlanta shows the difference between these two cities regarding cell sizes. Indeed, more data points have been obtained in larger distances in Atlanta than in Stockholm indicating larger cells in Atlanta.

These plots show that the median of rms delay spread does not tend to change at larger distances and it is similar for different base-mobile distances. Besides, the correlation coefficients of two data sets can quantitatively describe how correlated the two parameters are. This quantity is -0.0026 for Stockholm and -0.0838 for Atlanta which both evidence no correlation.

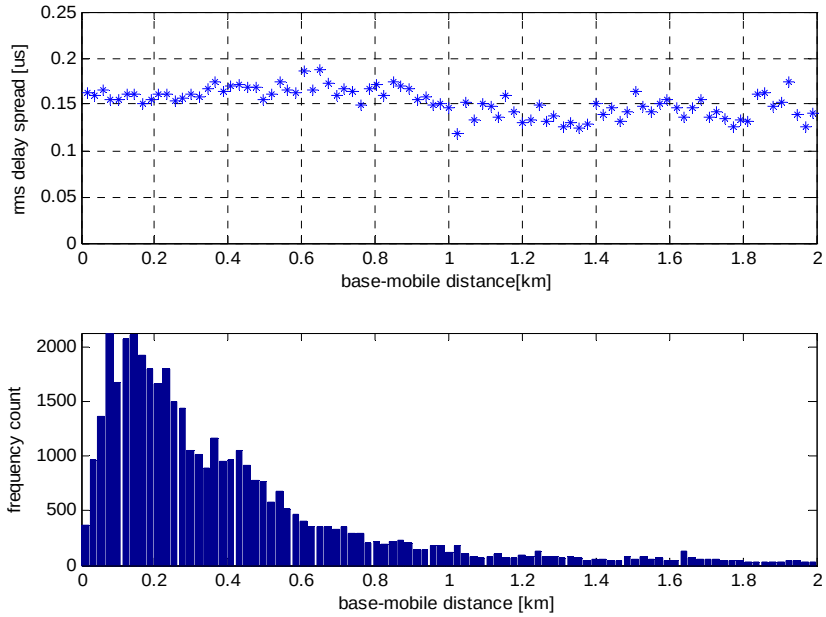

Figure 3-28: rms delay spread vs. base-mobile distance in Stockholm

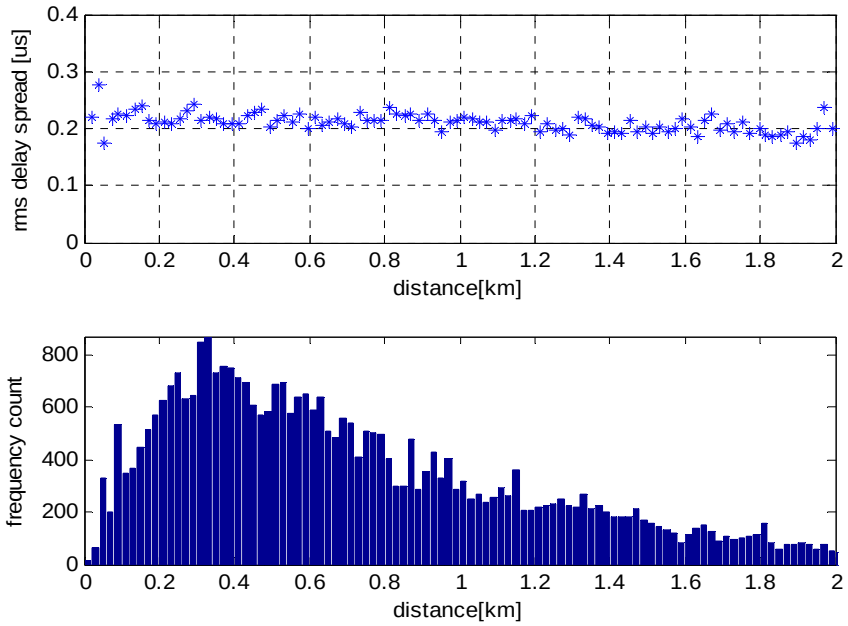

Figure 3-29: rms delay spread vs. base- mobile distance in Atlanta

One closer look at the delay spread GE paths can demonstrate that by getting further away from BSes, the rms delay spread does not necessarily grows. Figure 3-30 is such an example. The small circle shows the corresponding BS of the color coded path.

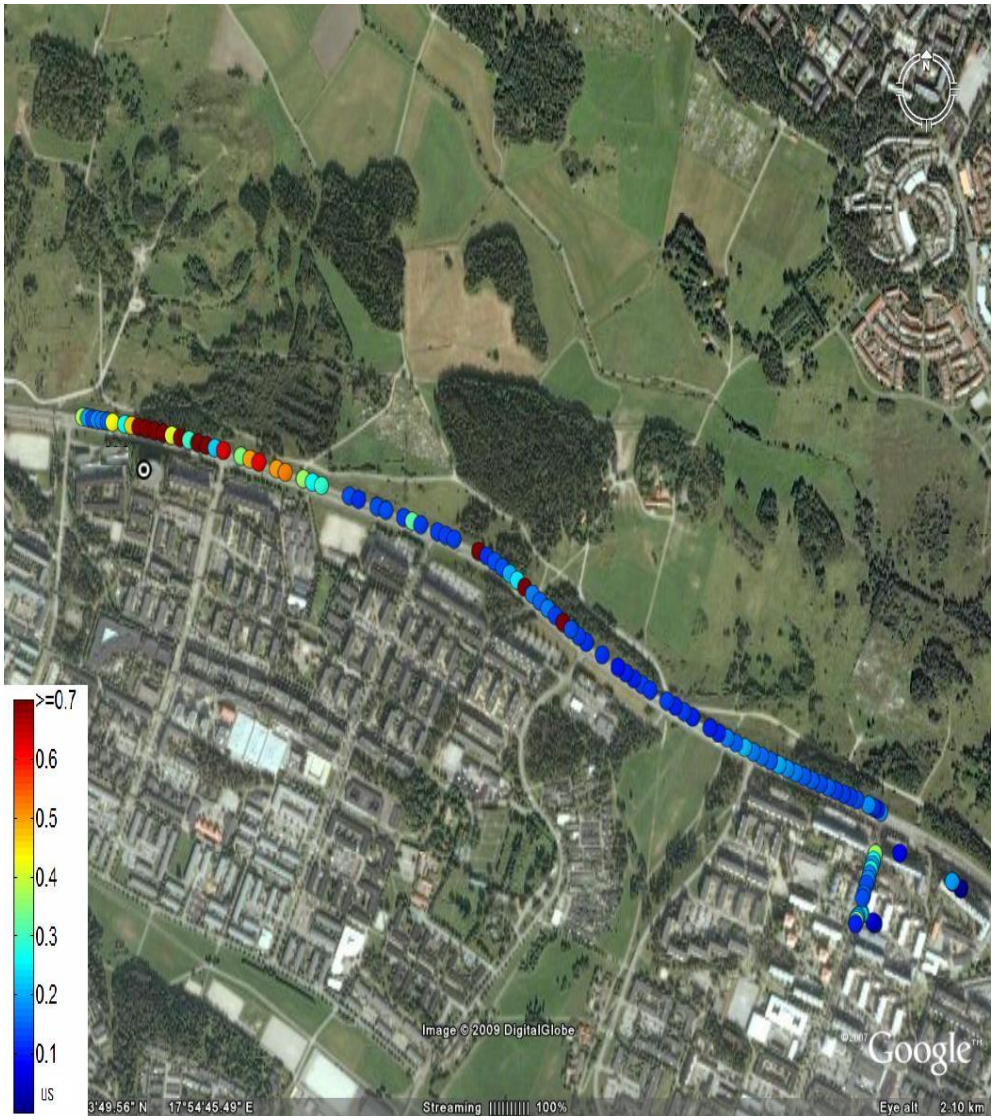

Figure 3-30: rms delay spread versus base-mobile distance, map size: $2 \times 2km$

It is worth mentioning that [7] discusses that the median rms delay spread increases with distance based on some older published measurement data. The main

explanation of [7] is that the power at lower delays caused by direct path and local scattering fall off sharply with base-mobile distance, while power at higher delays, due to distant reflections, fall off weakly with base-mobile distance.

However, if far away echoes caused by distant reflectors are rarely occurred, the above explanation may not be valid anymore. Indeed, *down-tilt* which is dominantly used in 3G networks might be a factor to reduce the echoes from distant scatterers. Down-tilt is pointing the antenna beam from the BS below the horizon to reduce the interference with neighboring cells.

3.3.5 rms delay spread versus RSCP

Another question which has been considered in some literatures such as [7], [8] is if there is any relationship between the rms delay spread and pathloss. As pathloss is related to RSCP by *Pathloss = Transmitted channel power* [*dBm*] - *RSCP* [*dBm*], the same concept can be questioned by considering RSCP. Therefore, the similar plots as above can be obtained by using RSCP and rms delay spread data sets from *3.3.5*. Figures 3-31 and 3-32 show rms delay spread versus RSCP plots from Stockholm and Atlanta measurements respectively. Here again each star presents the median of rms delay spreads within a RSCP interval of $1dBm$.

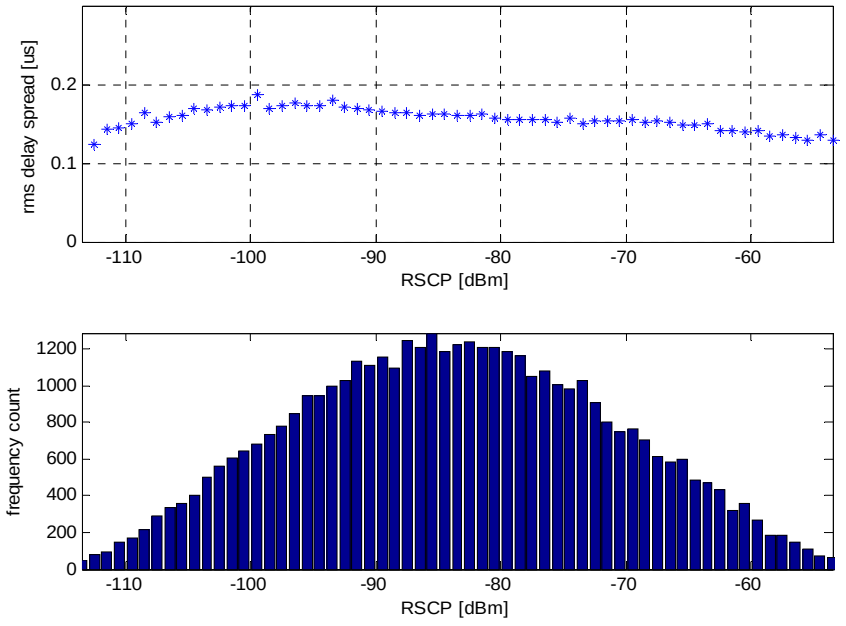

Figure 3-31: rms delay spread vs. RSCP in Stockholm

According to the plots, rms delay spread does not seem to change noticeably in different RSCP values and is almost similar for different RSCP values.

Moreover, the correlation coefficients of -0.0488 for Stockholm and -0.0033 for Atlanta represent how correlated the rms delay spread and RSCP are. Hence, these very low correlation confidents also indicate no evident correlation between the delay spread and distance.

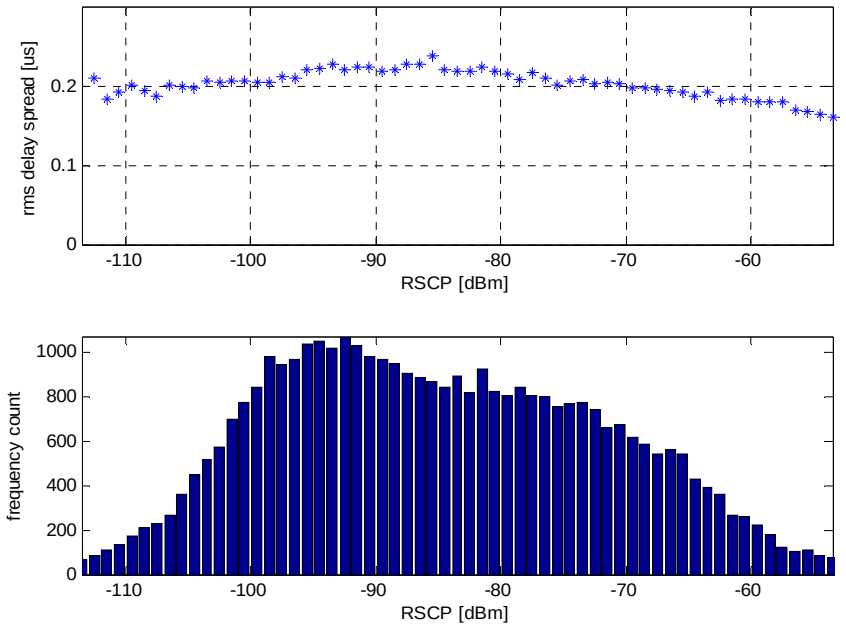

Figure 3-32: rms delay spread vs. RSCP in Atlanta

3.3.6 RSCP versus base-mobile distance

It is also interesting to know how RSCP values change by moving mobile terminal from the BS. So, the data sets of RSCP and base-mobile distance are plotted the same way as before to find out this relationship. Figures 3-33 and 3-34 are the resulted plots from Stockholm and Atlanta measurement data. Each star in the plots presents the median of RSCPes within 20 meters base-mobile distance.

The plots show that RSCP falls off as base-mobile distance increases. Similar results can be found in [8] and [10] for pathloss vs. distance.

We may also test how our data fits to a logarithm model such as Log-distance path loss model. The Log-distance path loss model is expressed as:

$$L = P_{TX}\ [dBm] - RSCP[dBm] = L_0 + 10\gamma \log_{10} \frac{d}{d_0} \quad (6)$$

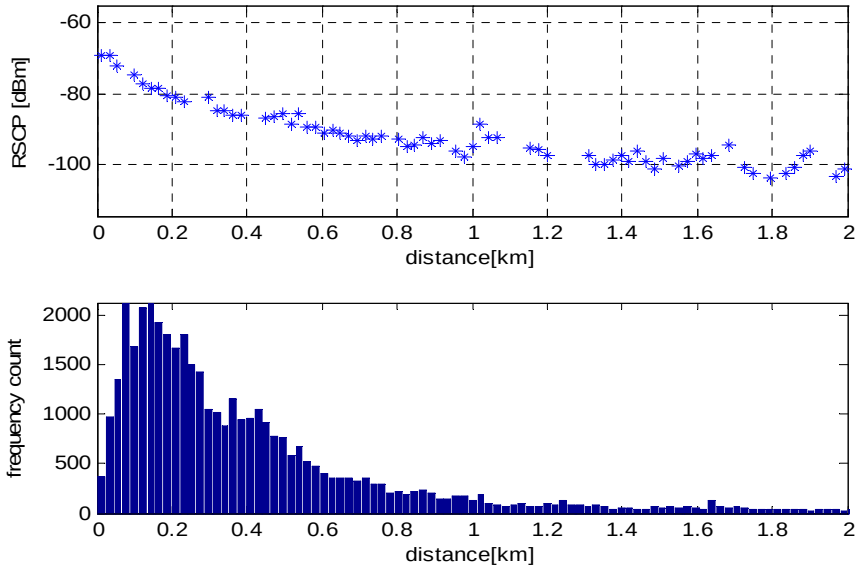

Figure 3-33: RSCP vs. base-mobile distance in Stockholm

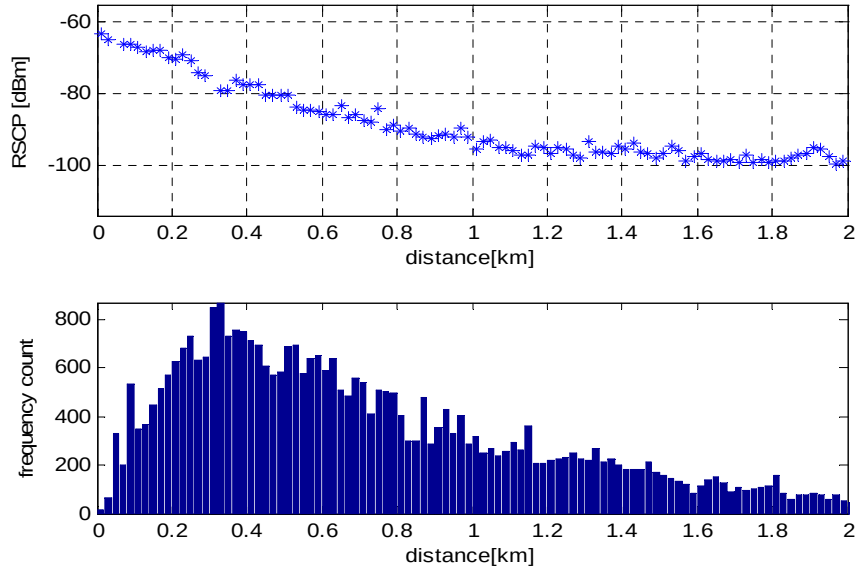

Figure 3-34: RSCP vs. base-mobile distance in Atlanta

Where, L is the total pathloss, P_{TX} is the transmitted power, L_0 is the pathloss at the reference distance d_0 and γ is the pathloss exponent. Simplifying the above model with emphasis on RSCP results in:

$$RSCP\left[dBm\right] = A + B\log_{10} d \qquad (7)$$

Where $A = P_{TX}[dBm] - L_0$, and $B = -\log_{10}\gamma$. Therefore, the data points are expected to form a straight line by plotting RSCP versus logarithm of distance. Figures 3-35 and 3-36 show such plots for Stockholm and Atlanta respectively with their corresponding histogram. As seen in the figures, both plots satisfy this expectation.

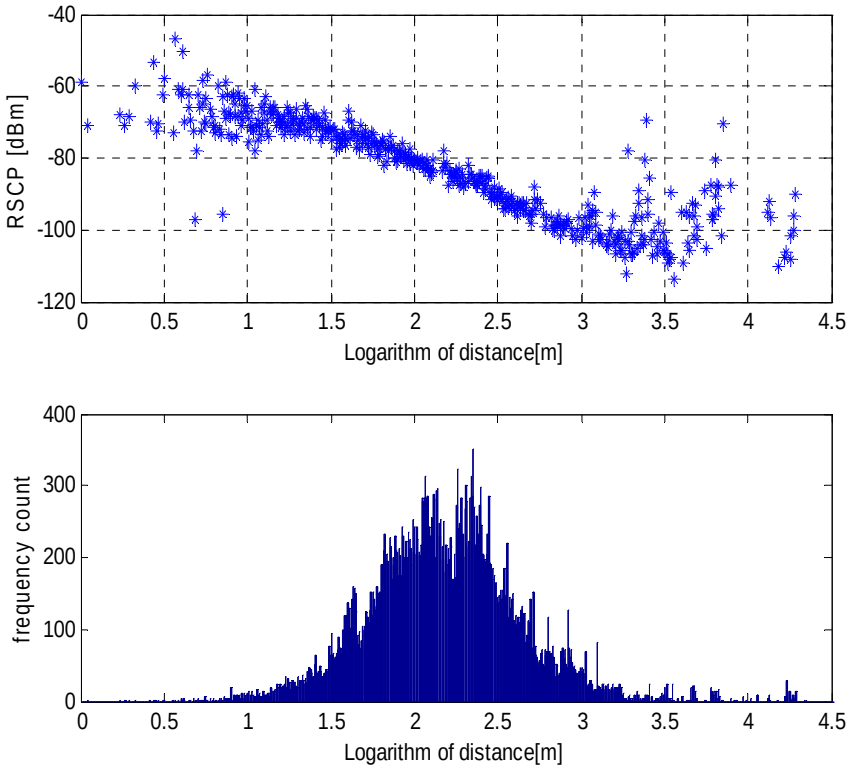

Figure 3-35: RSCP vs. logarithm of base-mobile distance for Stockholm data

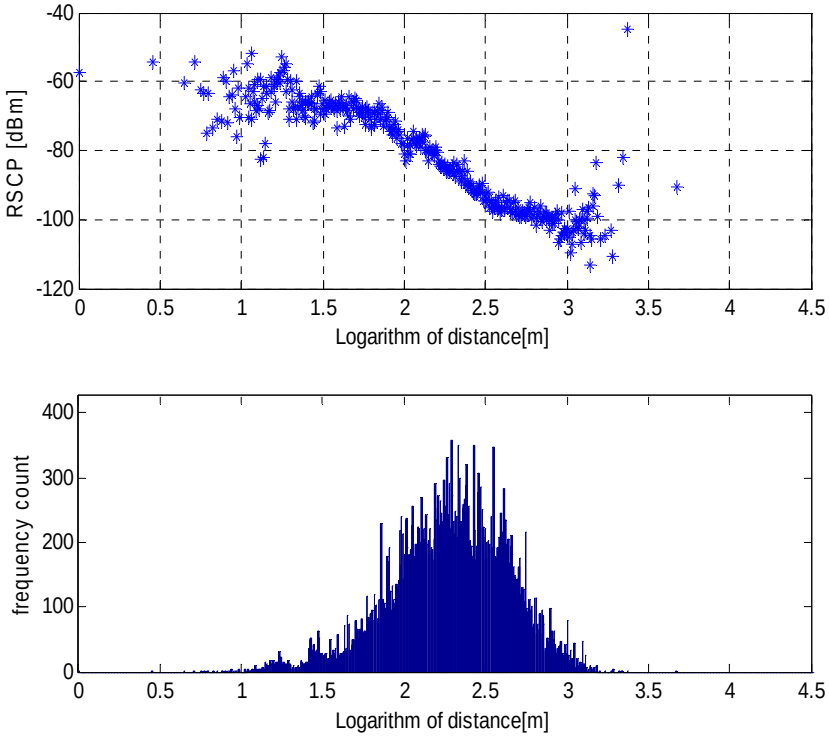

Figure 3-36: RSCP vs. logarithm of base-mobile distance for Atlanta data

The plots become scattered for very small or large distances where histograms also show small data sets of each bin. Therefore, to find a linear regression line the plots can be cleaned by removing the scattered part. The figures 3-37 and 3-38 show the same plots of 3-35 and 3-36 but with regression lines.

Besides, the slope of the lines, B, give the pathloss exponents which are $\gamma = 2.2$ and $\gamma = 3$ for Stockholm and Atlanta respectively. It should be mentioned these pathloss exponents may not be the pathloss exponents for a single cell since when the cell has good coverage more RSCP values are obtained compared to situation where the coverage is poor and other cells are received stronger.

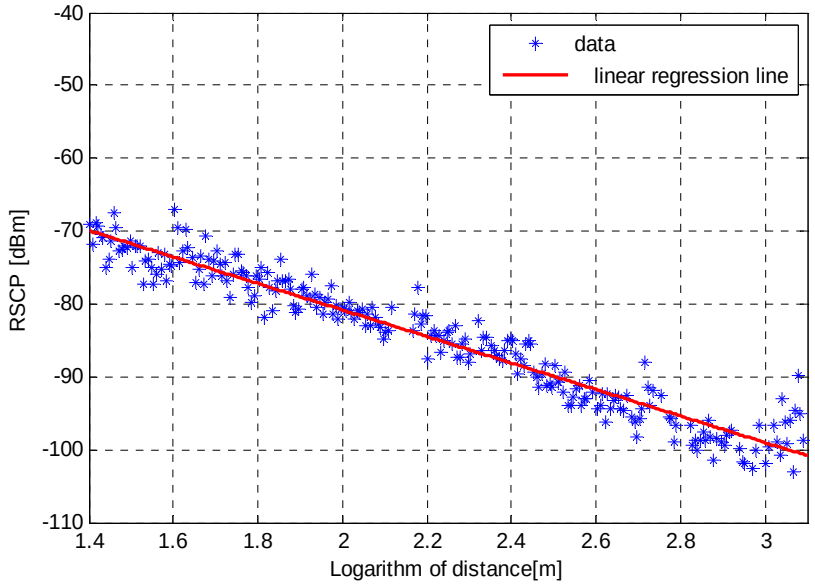

3-37: RSCP vs. Logarithm of distance for Stockholm data with regression line

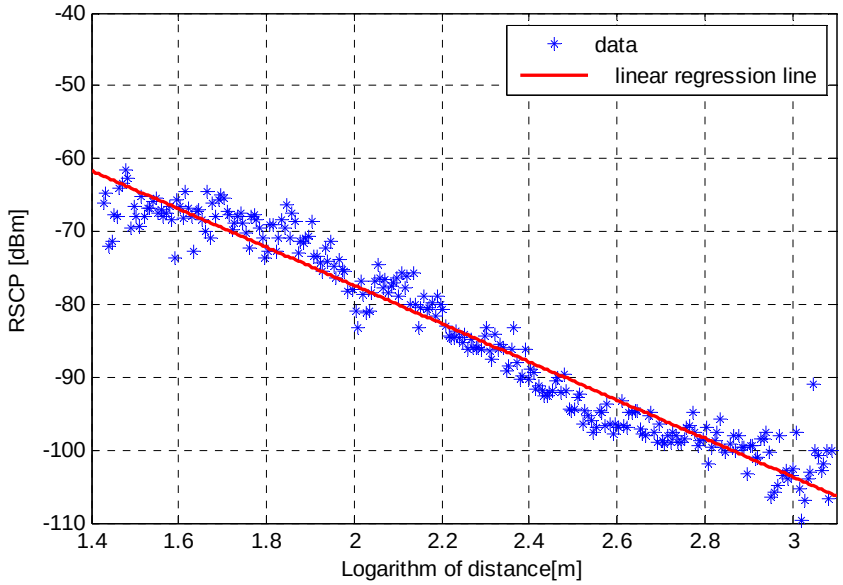

3-38: RSCP vs. Logarithm of distance for Atlanta data with regression line

3.3.7 Correlation of delay spread within and between sites

Another interesting feature that can be examined based on the measurement data is the correlation among the rms delay spreads derived from BSes in the same or different sites. Indeed, the question is if the delay spread of one BS in a specific site is high, is it then likely that the delay spread will be also high to the other BS of the same site or in other words how correlated the delay spreads are depending on their originating sites.

We have conducted some experiments to answer this question. At each experiment delay spreads which fulfill the conditions of the experiment are picked to be examined. The experiments details are as follows:

- *Experiment1 (same sites-same time):* in this experiment we pick the delay spreads derived from every two BSes (BS1, BS2) which are at the same site. Then, among the delay spreads of BS1 and BS2 those which have the same measurement time are grouped pairwise so that they can be compared. The pairwise delay spreads from all sites are then aggregated ($\sigma_{site1\cdots siteN}$).

$$\left.\begin{array}{l} site1 \rightarrow \sigma_{site1} = \begin{cases} BS1: \sigma_{rms,1}, \cdots, \sigma_{rms,k} \\ BS2: \sigma'_{rms,1}, \cdots, \sigma'_{rms,k} \end{cases} \\ \vdots \\ siteN \rightarrow \sigma_{siteN} = \begin{cases} BS1: \sigma_{rms,1}, \cdots, \sigma_{rms,n} \\ BS2: \sigma'_{rms,1}, \cdots, \sigma'_{rms,n} \end{cases} \end{array}\right\} \rightarrow \sigma_{site1\cdots siteN} = \begin{bmatrix} BS1: \sigma_{rms,1}, \cdots, \sigma_{rms,N} \\ BS2: \sigma'_{rms,1}, \cdots, \sigma'_{rms,N} \end{bmatrix}$$

- *Experiment2 (random sites-same time):* in this experiment we select the delay spreads which are derived from every two random BSes not at the same site. Again, the same as before those pair delay spreads with the same measurement time are picked and grouped.
- *Experiment3 (random sites-random time):* the delay spreads are selected from every two random BSes in this experiment the same way as experiment2. Then, among them some delay spreads from both BSes are randomly selected no matter if they have the same measurement time or not. Again, the selected delay spreads of each BS are grouped the same way as before.

Therefore, from each experiment one paired vector is achieved. The task is to find the correlation between each pair of values to realize how delay spreads are correlated to each other depending on their measured time and originating site.

One method to compute the correlation of each pair of delay spreads is to calculate the relative difference of them which is defined as:

$$d_r = \frac{\sigma'_{rms,BS1} - \sigma_{rms,BS2}}{mean(\sigma'_{rms,BS1}, \sigma_{rms,BS2})} \quad (8)$$

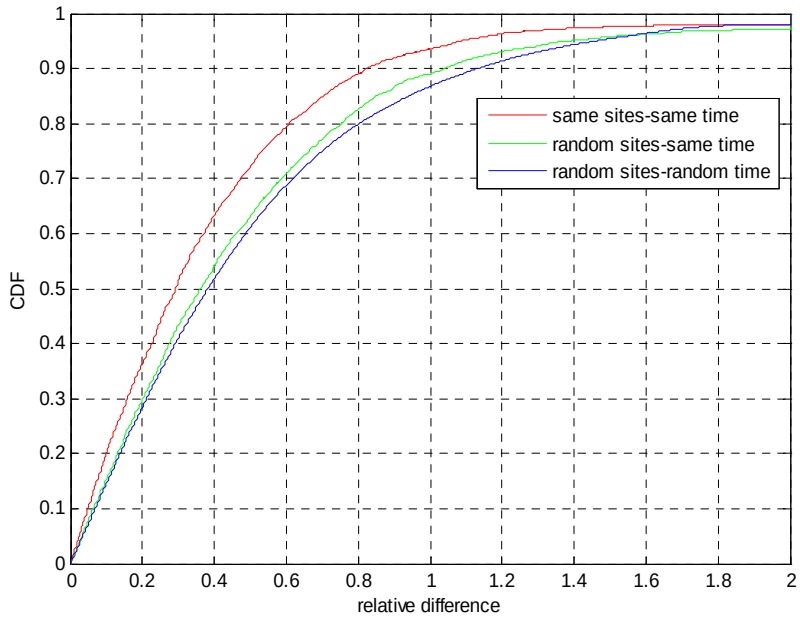

Figure 3-39: relative differences of 3 experiments

Computing the relative difference of paired rms delay spreads for each experiment gives a vector of values which can be complied as a CDF plot. Such CDF plots of three experiments are illustrated in the figure 3-39.

Another approach to find the correlation is computing the correlation coefficient of each pair of rms delay spreads. The computed correlation coefficients of explained experiments are as follows:

Experiment	Correlation coefficient
same sites-same time	0.34
random sites-same time	0.08
random sites-random time	0.007

Table 3-9: correlation coefficients of 3 experiments

From the figure 3-39, it can be observed that the relative difference values obtained for rms delay spreads associated with experiment 3 have slightly lower values. Also, the correlation coefficient of these rms delay spreads according to table 3-9 indicates a higher correlation. Hence, it seems that there is slightly more correlation between rms delay spreads derived from the same site compared to situation when delay spreads are originated from two different sites.

4 CONCLUSIONS AND DISCUSSION

In this thesis, extensive channel measurements were performed in various environmental types. The channel estimation was evaluated based on some lab measurements. We concluded that measurement results were quite trustful and accurate. Also, the rms delay spread distributions of the channels were studied after processing and classification of the raw data.

Generally, almost similar time dispersion properties were observed in Stockholm, Lille and New Orleans mostly due to their similar city structure and rather higher delay spread were noticed in Atlanta. The results also indicate that interestingly rms delay spread decreases consecutively from rural area to suburban and then to urban area in Stockholm city, while rms delay spread has higher values in urban than suburban area of Atlanta city. The possible forest effect on the time dispersion was proposed as an explanation of the high rms delay spreads observed in some rural vegetated areas.

Comparing our measurement results with current channel models indicated that time dispersion was significantly smaller than what was experienced in channel models such as 3GPP TU, GSM TU and SCM urban and it was larger than the channel models 3GPP RA and GSM RA delay spreads. However, our data was well fitted into SCM suburban model.

We also concluded that the median of rms delay spread does not tend to change at larger distances and it is similar for different base-mobile distances. Similarly, delay spread does not seem to change noticeably in different RSCP values and is almost similar for different RSCP values.

However, as expected the RSCP values declines as base-mobile distance increases. Furthermore, our data fitted to the Log-distance path loss model quite well and the path loss exponents of Stockholm and Atlanta cities were achieved by that. Moreover, a slight correlation between the rms delay spreads originated from the same sites was noticed in our attempts to find any dependency among rms delay spreads within and between sites.

4.1 Future work

One possible extension to this thesis can be performing more measurements to cover the areas such as hilly terrain or mountain areas that were not included in this thesis. It will be interesting to know the time dispersion properties of such channel models. Also, the results of these researches might be used in future for fine-tuning the channel models.

The conclusion of forest effect on delay spread has been regarded tentative due to uncertainty of scatterers identity. Hence, more investigations in this field are also suggested to be considered for future works. In addition, the relationship of delay

spread, base-mobile distance and RSCP can be tested by the help of more complicated statistical hypothesis testing to find out the exact probabilities of such relationships. Finally, one may conduct similar analysis as carried out in this thesis on other determining factors of time dispersion such as channel orthogonality factor.

APPENDIX A

The figure below shows the measured route in urban area of Stockholm by red paths. Urban area of Stockholm includes some islands connected to each other in the downtown.

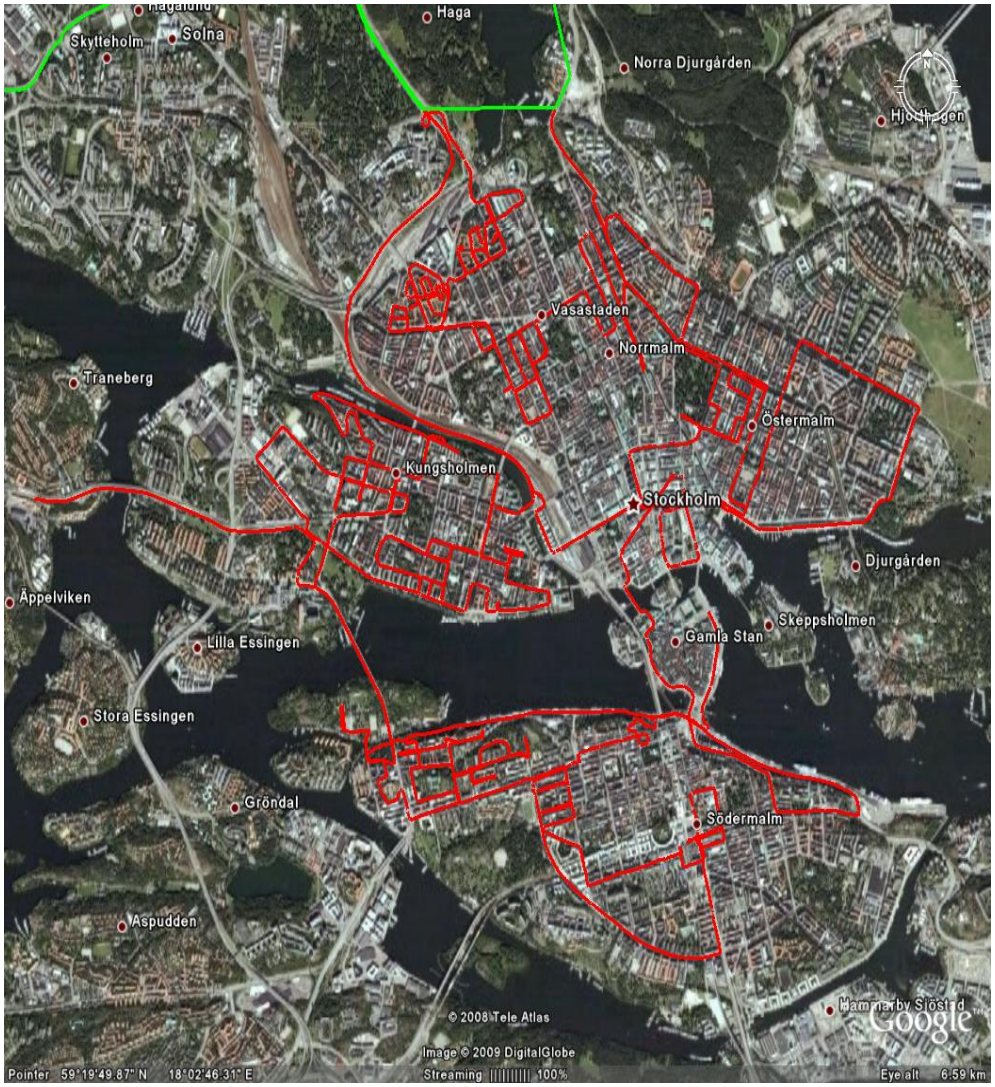

Figure 0-1: measured routes in urban area of Stockholm, map size: $8 \times 7 km$

The next figure shows the suburban area of the Stockholm by green color. Suburban area refers to area with more residential buildings out of the downtown having some open spaces. This area has less density than urban with larger cell sizes in the network.

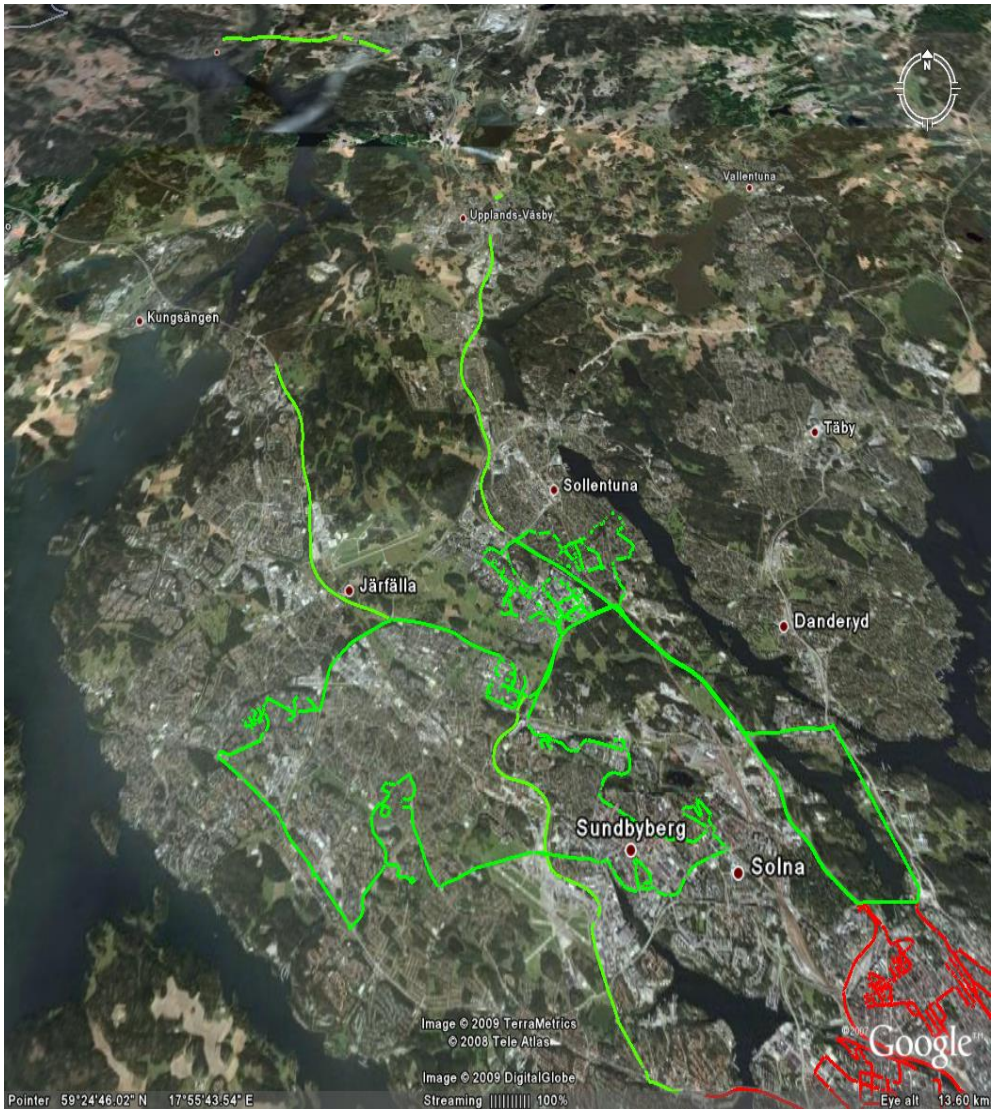

Figure 0-2: measured routs in suburban area of Stockholm, map size: $22 \times 35 km$

The measured route of rural area, the third considered area in Stockholm, is shown in purple path in the figure below. Rural areas are considered areas completely out of city with fields, open spaces or forests. It is almost free of residential buildings and the cell sizes are quite large.

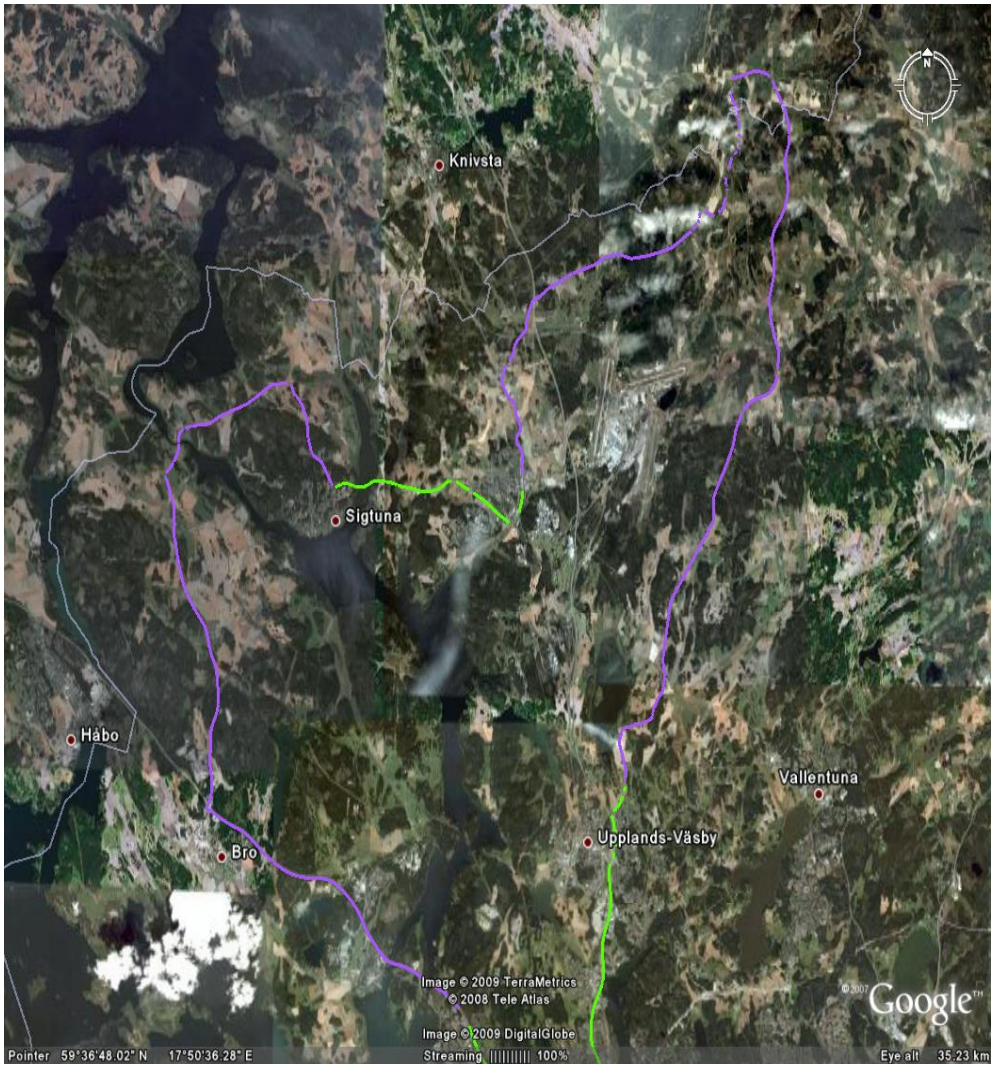

Figure 0-3: measured routes in rural area of Stockholm,
map size: $38 \times 34 km$

The following figure shows the measured routes in urban and suburban areas of Atlanta by red and green paths respectively.

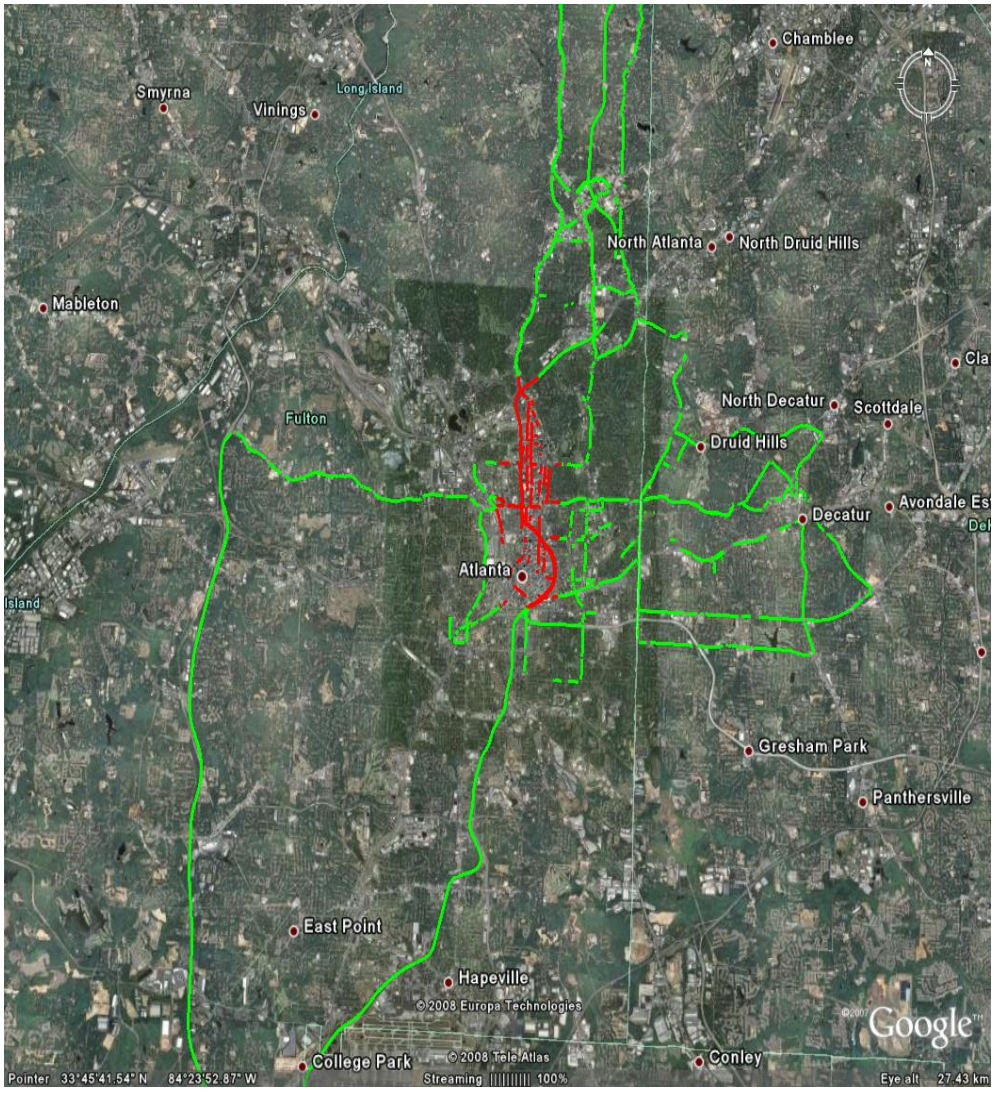

Figure 0-4: measured routes in urban and suburban areas of Atlanta, map size: $32 \times 28 km$

The wide-multi-lane highways in Atlanta were also interesting to consider separately. Therefore, the measurements data associated to highways were extracted and considered separately. In the figure below, the covered highways in the Atlanta campaign is illustrated by blue paths. It can be seen that highways are indeed a part of suburban area and also a small part of urban area.

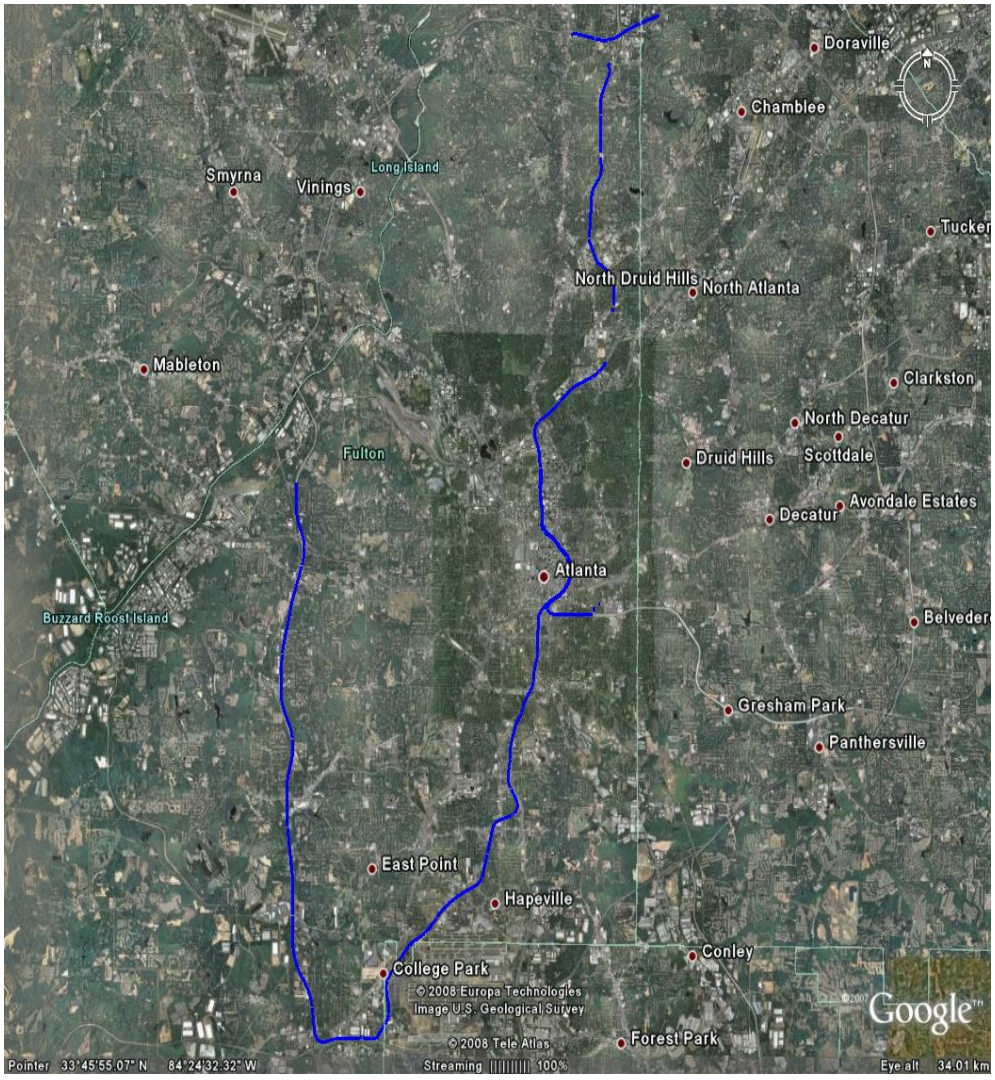

0-5: measured highways in Atlanta, map size: $39 \times 34 km$

REFRENCES

[1] K. Pahlavan and A. Levesque, *Wireless Information Networks*. New York: Wiley, 1995.

[2] H. Asplund, A. A. Glazunov, A. F. Molisch, K. Pedersen, and M. Steinbauer, "The COST 259 directional channel model part II: Macrocells," IEEE Transactions on Wireless Communications, vol. 5, no. 12, pp. 3434–3450, 2006.

[3] Rec. ITU-R M.1255, Guidelines for Evaluation of Radio Transmission Technologies for IMT-2000, International Telecommunication Union, Feb. 1997.

[4] 3rd Generation Partnership Project; Technical Specification Group Radio Access Networks; Deployment aspects (Release 7), 3GPP TR 25.943 V7.0.0.

[5] M.Tulldahl, "Evaluation of searcher techniques for an IS-95 based uplink," Ericsson Radio Systems AB, Kista, Sweden, Tech. Rep. T/U-97:367, 1997.

[6] H Holma and A. Toskala, WCDMA for UMTS-Radio Access For Third Generation Mobile Communications. New York: John Wiley & Sons, Ltd., 2001.

[7] L.J.Greenstein, V.Erceg, Y.S. Yeh, M.V.Clark," A new path gain/delay-spread propagation model for digital cellular channels", IEEE Transactions on vehicular Technology, Vol. 46, No. 2, May 1997, pp. 477-485.

[8] E.S. Sousa,V.M. Jovanovic, and C. Daigneault, " Delay spread measurements for the digital cellular channel in Toronto," IEEE Transactions on vehicular Technology, Vol. 43, pp. 837-847, Nov. 1994.

[9] A. S. Bajwa and J. D. Parsons, "Large area characterization of urban UHF multipath propagation and its relevance to the performance bounds of mobile radio systems," in Proc. Inst. Elect. Eng., vol. 132, pt. F, pp. 99–106, Apr. 1985.

[10] S. Y. Seidel et al., "Path loss, scattering and multipath delay statistics in four European cities for digital cellular and microcellular radiotelephone," IEEE Trans. Veh. Technol., vol. 40, pp. 721–730, Nov. 1991.

[11] 3rd Generation Partnership Project; Technical Specification Group GSM/EDGE Radio Access Network; Radio transmission and reception (Release 1999), 3GPP TS 05.05 V8.20.0, Annex C.3 Propagation models.

[12] 3rd Generation Partnership Project; Technical Specification Group Radio Access Networks; Spatial channel model for Multiple Input Multiple Output (MIMO) simulations(Release 6), 3GPP TR 25.996 V6.1.0.

[13] H. Asplund, K. Larsson, and P. Ökvist, "How typical is the"Typical Urban" channel model?," Vehicular Technology Conference. VTC 2008-Spring, May 2008.

[14] Y. de Jong, M. Herben, "A tree-scattering model for improved propagation prediction in urban microcells," IEEE Trans. on Vehicular Technology, Vol. 53, No. 2, pp. 503-513, March 2004.

[15] H. Asplund and J.-E. Berg, "Estimation of scatterer locations from urban array channel measurements at 1800 MHz," in Proc. RadioVetenskap och Kommunikation, June 1999, pp. 136-140.

[16] S. Kingsley and S. Quegan, Understanding Radar Systems. New York: McGraw-Hill, 1992.